ISSN 0915-633X

NATIONAL INSTITUTE FOR FUSION SCIENCE

Non-Taylor Magnetohydrodynamic Self-Organization

Shao-ping Zhu, R. Horiuchi, T. Sato and
The Complexity Simulation Group

(Received - Oct. 4, 1994)

NIFS-314 Oct. 1994

RESEARCH REPORT
NIFS Series

NAGOYA, JAPAN

NON-TAYLOR MAGNETOHYDRODYNAMIC SELF-ORGANIZATION

Shao-ping Zhu[1], Ritoku Horiuchi,[1,2] and Tetsuya Sato[1,2]

and

The Complexity Simulation Group[2,†]

[1] Department of Fusion Science, The Graduate University for Advanced Studies,

Nagoya 464-01, Japan

[2] Theory and Computer Simulation Center, National Institute for Fusion Science,

Nagoya 464-01, Japan

Abstract

A self-organization process in a plasma with a finite pressure is investigated by means of a three-dimensional magnetohydrodynamic simulation. It is demonstrated that a non-Taylor finite β self-organized state is realized in which a perpendicular component of the electric current is generated and the force-free(parallel) current decreases until they reach to almost the same level. The self-organized state is described by an MHD force-balance relation, namely, $\mathbf{j}_\perp = \mathbf{B}\times\nabla p/\mathbf{B}\cdot\mathbf{B}$ and $\mathbf{j}_\parallel = \mu\mathbf{B}$ where μ is not a constant, and the pressure structure resembles the structure of the toroidal magnetic field intensity. Unless an anomalous perpendicular thermal conduction arises, the plasma cannot relax to a Taylor state but to a non-Taylor(non-force-free) self-organized state. This state becomes more prominent for a weaker resistivity condition. The non-Taylor state has a rather universal property, for example, independence of the initial β value. Another remarkable finding is that the Taylor's conjecture of helicity conservation is, in a strict sense, not valid. The helicity dissipation occurs and its rate slows down critically in accordance with the stepwise relaxation of the magnetic energy. It is confirmed that the driven magnetic reconnection caused by the nonlinearly excited plasma kink flows plays the leading role in all of these key features of the non-Taylor self-organization.

Keywords: magnetohydrodynamic simulation, finite pressure, magnetic helicity, driven magnetic reconnection, stepwise relaxation, non-Taylor self-organization

---

[†]K.Watanabe, T.Hayashi, Y.Todo, T.H.Watanabe, A.Kageyama and H.Takamaru

I. Introduction

In the last two decades, Taylor's theory[1-2] has attracted considerable attention of plasma physisists, because it has been able to predict a stable magnetic structure, for example, the field reversal structure of the reversed field pinch(RFP) and the spheromak configuration. Taylor conjectured that a weakly resistive magnetohydrodynamic(MHD) plasma tends to evolve toward a minimum magnetic energy state under the constraint of the total magnetic helicity conservation, and predicted that a self-organized state(minimum magnetic energy state) is a force-free equilibria $\mathbf{j} = \mu\mathbf{B}$ where μ is a constant eigenvalue that determines the minimum energy.

Many numerical simulations [3-10] have been carried out to confirm the Taylor's conjecture and revealed the dynamical behavior of the self-organization process. Through a three-dimensional full MHD simulation study Horiuchi and Sato[6-7] demonstrated that the nonlinear driven magnetic reconnection plays a key role in the self-organization process of an MHD plasma. For instance, through the nonlinear driven magnetic reconnection process the spectrum of the magnetic energy exhibits a normal cascade, while that of the magnetic helicity does an inverse cascade. An explanation of the phenomenon that the dissipation rate of the magnetic energy is faster than the corresponding rate for the magnetic helicity is also given in terms of the driven reconnection process.

It should be remembered, however, that the Taylor's theory can be applied to a case where the plamsa pressure is kept uniform throughtout the whole system. In view of the fact that in self-organization an excess free magnetic energy is transformed into the thermal energy, it is not a natural consequence that the plasma pressure becomes homogeneous. If the thermal energy, when produced, is immediately expulsed by some processes such as radiation, or if the plasma is not thermally insulated perpendicular to the magnetic field, then the homogeneity condition can be realized. Otherwise, this condition would not be met. Many efforts have been made to extend the Taylor's theory to

a finite pressure MHD plasma[11-12]. However, most of the works have reached to the Taylor's force-free state. Recently, Kondoh et al[13] have dealt with this problem from a different viewpoint and asserted that the self-organized state becomes a non-force-free one if the electrical resistivity has a spatial dependence. For the spatially uniform electrical resistivity, their state is degenerated into the Taylor state. Numerical simulation is a good methodology to understand the self-organization process of a finite pressure MHD plasma. A three-dimensional simulation study of Horiuchi and Sato[8] showed that a finite pressure MHD plasma relaxed toward a Taylor's force-free minimum energy state. We suspected that the homogenization of the pressure might have been caused mainly by the numerical diffusion and partially by the choice of the boundary condition that the pressure is floating.

In an attempt to bring out clearly the effect of the plasma pressure on the self-organization process of an MHD plasma, we employ the three-dimensional MHD simulation code[14] with a fourth-order accuracy both in time and space. The plan of the paper is as follows. In Sec.II we explain our simulation model. The simulation results are presented in Sec.III. The section IV contains a brief summary of the present study.

II. Simulation Model

We consider a compressible dissipative MHD plasma with a finite pressure confined in a conducting cylindrical vessel with a rectangular cross-section. The basic equations are described in the dimensionless form as

$$\frac{\partial \rho}{\partial t} = -\nabla \cdot (\rho \mathbf{v}), \tag{1}$$

$$\frac{\partial \mathbf{F}}{\partial t} = -\nabla \cdot (\mathbf{F}\mathbf{v}) - \nabla p + \mathbf{j} \times \mathbf{B}, \tag{2}$$

$$\frac{\partial \mathbf{B}}{\partial t} = \nabla \times (\mathbf{v} \times \mathbf{B} - \eta \mathbf{j}), \tag{3}$$

$$\frac{\partial p}{\partial t} = -\nabla \cdot (p\mathbf{v}) + (\gamma - 1)(-p\nabla \cdot \mathbf{v} + \eta \mathbf{j} \cdot \mathbf{j}), \tag{4}$$

where

$$\mathbf{j} = \nabla \times \mathbf{B}, \tag{5}$$

and $\mathbf{F}(= \rho \mathbf{v})$ is the mass flux density, p is the thermal pressure, ρ is the mass density, $\mathbf{v}$ is the fluid velocity, $\mathbf{B}$ is the magnetic field, $\mathbf{j}$ is the current density, η is the uniform electrical resistivity, and $\gamma(= 5/3)$ is the ratio of the specific heats. In general, the thermal conduction term should be added in Eq. (4). In this paper, however, we consider the case where its effect is discarded and the vessel is thermally insulated.

A Cartesian coordinate system (x, y, z) is employed. The system is periodic along the z-axis with a periodic length L_t, and is surrounded by a conducting wall at $x = 0$ and L_p, and $y = 0$ and L_p, i.e., $\mathbf{n} \cdot \mathbf{v} = 0$, $\mathbf{n} \times \mathbf{j} = 0$ and $\mathbf{n} \cdot \mathbf{B} = 0$, where $\mathbf{n}$ is the unit vector normal to the conducting surface. As an initial condition we impose a two-dimensional force-free equilibrium which is given by

$$B_x = [k_1 B_1 \sin(k_2 x)\cos(k_1 y) + k_2 B_2 \sin(k_1 x)\cos(k_2 y)]/k_0, \tag{6}$$

$$B_y = -[k_2 B_1 \cos(k_2 x)\sin(k_1 y) + k_1 B_2 \cos(k_1 x)\sin(k_2 y)]/k_0, \tag{7}$$

$$B_z = B_1 \sin(k_2 x)\sin(k_1 y) + B_2 \sin(k_1 x)\sin(k_2 y), \tag{8}$$

$$\rho = \rho_0, \; p = p_0, \tag{9}$$

where ρ_0 and p_0 are constant, $k_0 = \sqrt{k_1^2 + k_2^2}$, $k_1 = n_1\pi/L_p$, $k_2 = n_2\pi/L_p$, n_1 and n_2 are integers.

There are three important parameters to characterize the energy relaxation process of an MHD plasma, i.e., (a) the initial normalized magnetic helicity α ($= 2\pi L_p K/L_t\psi^2$), (b) the initial normalized magnetic energy ϵ ($= L_p W/2K$), and (c) the plasma beta β ($= 4p_0/(B_1^2 + B_2^2)$), where K and W are the total magnetic helicity and energy, respectively,

and ψ ($= \int B_z dxdy$) is the total toroidal magnetic flux. In our system these values are described by the parameters n_1, n_2, L_t/L_p, B_1, B_2, and p_0.

The Taylor's relaxation theory[1,7,15] predicts that the plasma with $\alpha > \alpha_c (= 8.21)$ relaxes to a helically symmetric state where the pressure is uniform and the toroidal mode number n of the helical plasma column is determined by the ratio of the side lengths L_t/L_p. For example, for the initial condition that $n_1 = n_2 = 3$,$B_1 = 1$, $B_2 = 0$, and $L_t/L_p = 3$, hence, $\alpha = 58.3$, $\epsilon = 6.7$, it is expected that the system relaxes to a helically symmetric force-free state with the toroidal mode number $n = 1$ and $\epsilon = 3.1$. The MHD simulation study of Horiuchi and Sato[7] demonstrated that the plasma relaxed to a helical state with a minimum energy state expected from the relaxation theory.

The numerical simulation of Horiuchi and Sato was based on the two-step Lax-Wendroff method. This method is known to numerically smooth away the high wavenumber components, so that the numerical diffusion may mask a significant fine structure of a real phenomenon and sometimes lead us to an erroneous conclusion. In order to reduce the numerical artifact and produce a physically reliable result we use a high-precision simulation code[14] which relies on an explicit finite-difference method with fourth-order accuracy both in space and time. This method ensures a reasonably reliable discussion on the subtleties of the structure development due to the effect of finite plasma pressure. The simulation domain is implemented on a ($100 \times 100 \times 150$) point grid.

III. Simulation Results

The initial magnetic field configuration is given by Eqs.(6)-(8) where we have chosen as $n_1 = n_2 = 3$, $L_t/L_p = 3$, $B_1 = 1$, and $B_2 = 0$ (see, Ref.7). The density and pressure are initially distributed uniformly, as is given by Eq.(9). Figure 1 shows the vector plots of the poloidal magnetic field (right) and the contour plots of the toroidal magnetic field intensity(left) in the poloidal plane (x, y) in the initial stage. In the following discussion,

we devote ourselves to the analysis of the simulation result for Case A given in Table-1 unless otherwise stated.

A. Fundamental properties of energy relaxation

The previous papers[7-10] have revealed two important characteristics of the MHD self-organization, namely, (1) conservation of the magnetic helicity and the selective dissipation of the magnetic energy, (2) the normal cascade of the magnetic energy spectrum and the inverse cascade of the magnetic helicity spectrum. Figure 2 shows the temporal evolutions of the total magnetic energy W (solid line) and the total magnetic helicity K (dashed line) normalized by their initial values. There appear two relaxation phases in the temporal evolution, i.e., the first relaxation phase ($18t_A < t < 25t_A$) and the second relaxation phase ($35t_A < t < 46t_A$). The magnetic energy dissipates rapidly in the relaxation phases in the time scale comparable to the Alfven transit time, while the magnetic helicity decreases slowly in a resistive time scale without suffering any influence during the whole simulation. In other words, the selective dissipation takes place in two steps for the magnetic energy in the present example.

The selective dissipation can be explained in terms of the spectral transfer[6-8]. Figure 3 shows the temporal evolutions of the average wavenumber of the energy spectrum (solid line) and that of the helicity spectrum (dashed line). It is clear in Fig. 3 that the energy spectrum is transferred to a higher wavenumber region (normal cascade), while the helicity spectrum is transferred to a lower wavenumber region (inverse cascade). Because of these normal and inverse cascades for the magnetic energy and helicity, one can apparently understand the selective dissipation for the magnetic energy and the conservation of the magnetic helicity. These results are in good agreement with the simulation results obtained in the previous papers[6-9].

The selective dissipation is closely related to the nature of magnetic reconnection in

real space. From the MHD equations (1)-(4), the total magnetic energy and the total magnetic helicity decrease according to the following relations:

$$\frac{dW}{dt} \simeq -\eta \int \mathbf{j} \cdot \mathbf{j} d^3\mathbf{x}, \tag{10}$$

and

$$\frac{dK}{dt} = -\eta \int \mathbf{j} \cdot \mathbf{B} d^3\mathbf{x}. \tag{11}$$

If the force-free relation $\mathbf{j} = \mu\mathbf{B}$ holds, both the magnetic energy and the magnetic helicity must dissipate in a similar fashion. The existence of selective dissipation indicates, therefore, that the dissipation structure (or the current profile) during the relaxation must be largely different from the force-free one. Figure 4 shows the temporal evolutions of the total energy dissipation D_W and the total helicity dissipation D_K where $D_W = \int (\mathbf{j} \cdot \mathbf{j}) d^3\mathbf{x}$ and $D_K = \int (\mathbf{j} \cdot \mathbf{B}) d^3\mathbf{x}$. In the initial phase ($0 < t < 18 t_A$) these quantities decrease with the same dissipation rate. This means that the force-free relation approximately holds in this period. The energy dissipation tends to increase drastically as soon as the first and second relaxations set in, and its value becomes much larger than that expected from the force-free state.

On the other hand, the evolution curve of the helicity dissipation drops abruptly to a much lower level than that expected from the force-free state as soon as each relaxation phase starts. These phenomena are in good correlation with the normal cascade of the energy spectrum and the inverse cascade of the helicity spectrum in the Fourier space, which are both proportional to the square of the wavenumber. The stepwise drop of the dissipation rate of the magnetic helicity gives us a new fact that the Taylor's conjecture of helicity conservation is, in a strict sense, not satisfied. Instead, the helicity dissipation exhibits a slowing-down behavior, which is opposite to the acceleration of the dissipation rate of the magnetic energy, as is evident in Fig.4.

Let us then examine how the dynamics leading to the selective dissipation is going on. Figure 5 shows the vector plots of the poloidal velocity (v_x, v_y) (top-left), the contour

maps of the toroidal magnetic filed B_z (top-right), toroidal electric current j_z (bottom-left) and pressure p (bottom-right) in the poloidal cross-section ($z = L_z/2$) at the time of $t = 18t_A$. We note that the contour with a negative value of B_z or j_z and the contour less than the average value of p are plotted by a dotted line. Magnetic reconnection takes place at two positions in a poloidal plane , one at a contact point of two negative toroidal fluxes and the other at a contact point of two positive toroidal fluxes, as is observed from the directions of the induced flow arrows in Fig.5. The converging plasma flows directing towards the two reconnecton points, which are created by an ideal kink instability, result in the local enhancement of the electric current density (see, the bottom-left panel of Fig. 5), thus increasing the dissipation rate of the magnetic energy. In this way the kink flow-driven magnetic reconnection is stimulated and a fast transfer of the magnetic energy to the thermal energy is realized.

It is interesting to note that magnetic reconnection develops in a saddle point of the toroidal magnetic field where it is null. A careful examination of the results reveals that the direction of the toroidal electric current is antiparallel to the direction of the toroidal magnetic field in the vicinity of the reconnection point ($j_z B_z < 0$), although the initial value of $j_z B_z$ is positive everywhere in the force-free configuration. This ensures that the dissipation rate of the total helicity is reduced. Incidentally, it should be noted that the contours of the reconnection current clearly exhibit an X-type structure.

Figure 6 shows the bird's-eye views of the profiles of $\mathbf{j} \cdot \mathbf{j}$ (top) and $-\mathbf{j} \cdot \mathbf{B}$ (bottom) in the poloidal cross-section ($z = L_z/2$) at the time of $t = 20.43t_A$, where only the negative part of $\mathbf{j} \cdot \mathbf{B}$ is displayed in the bottom panel for clarity. One can see the value of $\mathbf{j} \cdot \mathbf{j}$ is anomalously large in the vicinity of the reconnection points, but $\mathbf{j} \cdot \mathbf{B}$ has negative peaks there. It is also noted that the height of the highest peak of negative $\mathbf{j} \cdot \mathbf{B}$ is larger than that of positive $\mathbf{j} \cdot \mathbf{B}$. This ensures that driven reconnection acts to anomalously enhance the dissipation of the magnetic energy, but, on the contrary, to reduce the dissipation of

the magnetic helicity, which is consistent with Fig.4. It should be noted that reconnection can take place at a saddle point of the toroidal magnetic field intensity contour between the facing positive islands or the negative islands. In either reconnection the reconnection current is opposite to the toroidal current, hence, the toroidal field of the reconnection islands, so that, $\mathbf{j} \cdot \mathbf{B} < 0$ in the vicinity of the reconnection point. This result is important and new in the sense that the Taylor's conjecture of the magnetic helicity conservation during the relaxation process is not valid, in a strict sense.

B. Finite β self-organization

Let us now go on to the study of the self-organized structure in a finite pressure (β) MHD plasma. Let us examine the simulation data with particular attention to whether the Taylor state is realized in the final state or not. Figure 7 shows the contour maps of the toroidal magnetic field (top), and the pressure (bottom) at $t = 19.0t_A$ (left), $t = 32.4t_A$ (middle), and $t = 71.3t_A$ (right) for $\beta = 0.6$ and $\eta = 5 \times 10^{-4}$ (Case C) where the red color stands for a contour larger than the average value of the pressure(lower part) and the positive toroidal magnetic field (upper part). It is evident that a clear structure is created in the pressure distribution as the magnetic structure is deformed, exhibiting a good resemblance between the two.

We note that there are two processes that lead to the increase in the thermal pressure; the first one is the fast heating process which is assocoated with driven magnetic reconnection, and the second is the slow heating process which is governed by the resistive diffusion process prior to the onset of reconnection. In the early phase ($0 < t < 18t_A$), the magnetic field intensity decreases in the resistive time scale, while keeping the same spatial pattern as the initial current pattern $\mathbf{j} \parallel \mathbf{B}$, hence, the magnetic field one. Therefore, the spatial structure of the pressure created through the ohmic heating becomes similar to that of the initial current pattern and , equivalently, to that of the magnetic

field pattern (left panels). This heating process is the slow process in which the amount of the enhanced heat is determined by the value of the electrical resistivity.

The development of an ideal kink instability deforms the magnetic flux tube in a helical fashion and increases the electric current at the contact point(or line) between the approaching magnetic flux tubes. Driven magnetic reconnection sucessively combines two negative flux tubes into one negative flux tube and two positive flux tubes into one positive, and, subsequently. the four original negative tubes are merged into one big one in the central part and the five original positive tubes become four tubes on the four corners in the first relaxation phase(upper middle panel in Fig.7). This process is the fast one in which a rapid transfer of the magnetic energy to the thermal energy is carried out. Since reconnection takes place at a local minimum point of the original force-free current, the pressure profile generated by this driven magnetic reconnection process is peaked at the local minimum point of the pressure profile generated by the early slow process. The enhanced pressure-gradient force(slow shock) generates fast outflows whereby the thermal energy and the reconnected magnetic flux are carried away along the field line from the reconnection point, thus, the pressure structure is aligned along the field line.

Thereafter, the second relaxation takes place and the four positive flux tubes are merged into one flux tube through the driven magnetic reconnection process occuppying the upper-left half region, while the big negative flux tube is pushed towards the bottom-right corner(the right panel in Fig. 7). It is important to point out that even in the final stage the pressure maintains a clear structure similar to the magnetic structure.

Since the kink and reconnection flows transverse to the field lines are relatively small and decay after the second relaxation, the localized structure of the thermal pressure obtained is sustained for a fairly long time. Figure 8 shows the temporal evolution of the pressure deviation from the average δp defined by

$$\delta p = \left\{ \frac{< (p - < p >)^2 >}{< p >^2} \right\}^{1/2} \tag{12}$$

for three different resistivities, namely, Cases A (solid line), B (dashed line), C(dot-dashed line) in Table 1, where $< f(\mathbf{x}) >$ stands for the average of $f(\mathbf{x})$ over the whole volume. The pressure deviation increases slowly in the early quiet phase and its rate becomes enhanced suddenly as soon as the first relaxation sets in. This sudden increase is due to the fast relaxation process and its time scale is a few times of the Alfven transit time. It is worthy to note that the enhancement of the pressure deviation becomes more conspicuous as the resistivity decreases in the fast process, in contrast to the fact that the pressure deviation is enhanced in proportion to the resistivity in the slow process. This phenomenon can be easily explained by considering the nature of driven reconnection.

In driven reconnection[16-18] the reconnection current j_{rec} is roughly given by equating the reconnection electric field ηj_{rec} to the driving electric field E_d. The transfer rate of the magnetic energy to the thermal energy, ηj_{rec}^2, is given as E_d^2/η, which indicates the inverse proportionality to the resistivity, since E_d which gives the convection flow of the ideal kink instability is almost independent of η. The energy transfer rate of the fast process is consequently enhanced and is proportional inversely to the resistivity, while that of the slow diffusion process is proportional to the resistivity, as is evident in Fig.8.

After the second relaxation, the pressure deviation decays gradually according to the resistive diffusion time scale. The pressure deviation δp, however, keeps a finite level even in the final period of the simulation, as is seen in Fig.8. It is to be noted that the magnetic energy is much smaller than the thermal energy in the final self-organized state. Thus, the pressure deviation remains sizable and meaningful, though apparently small.

We shall now examine the effect of the pressure gradient and clarify whether the force-free condition is satisfied in the relaxed state of the finite beta plasma. Let us split the electric current into the force-free (parallel) component and the perpendicular component. Figure 9 shows the temporal envolutions of the normalized parallel component $J_{||}$ and the normalized perpendicular component $J_{\perp}$ of the electric current for Cases A

(solid line), B (dashed line), C(dot-dashed line), where $J_{\parallel} =< |\mathbf{j}_{\parallel}|/|\mathbf{j}| >$, $J_{\perp} =< |\mathbf{j}_{\perp}|/|\mathbf{j}| >$, $\mathbf{j}_{\parallel} = (\mathbf{j}\cdot\mathbf{B})\mathbf{B}/(\mathbf{B}\cdot\mathbf{B})$, and $\mathbf{j}_{\perp} = \mathbf{j} - \mathbf{j}_{\parallel}$. The perpendicular component increases rapidly in accordance with the growth of the ideal kink instability in the first relaxation phase. After some period it increases again in the second relaxation phase and reaches comparable to the parallel component. The amplitude attained is almost maintained during the entire period of simulation run. This result suggests that the system relaxes to an equilibrium state that is absolutely different from the force-free state.

C. Non-Taylor relaxation

We are now in a position to elucidate the structure which is realized in an MHD plasma in the presence of the thermal pressure, and the nature which is different from what is predicted by the Taylor's conjecture for the zero β case. Figure 10 shows a three-dimensional display of the isosurfaces of the toroidal magnetic field at $t = 0$,$t = 19.0t_A$,$t = 32.4t_A$, and $t = 71.3t_A$ for Case C where the yellow and red isosurfaces stand for the positive toroidal flux and the negative toroidal flux, respectively. There exist five positive flux tubes and four negative flux tubes at $t = 0$. This spatial structure is deformed into an intermediate one with one negative helical flux tube and four positive flux tubes through the driven magnetic reconnection process in the first relaxation phase. Finally, the system self-organizes into a helically symmetric state of the toroidal mode number $n = 1$ in which one positive helical flux tube and one negative flux tube exist. At a glance this simulation result may appear similar to the self-organized state expected from the relaxation theory for the zero beta plasma.[15] As mentioned above, however, the spatial structure of the thermal pressure is not uniform even at the final stage and hence the final equilibrium state is considered to be different from the force-free one.

In view of the fact that the pressure is not uniform, notwithstanding its apparent similarity to the Taylor state, there must exist some crucial difference from it. In spite

of the apparent similarity between some of the present results for finite β with those expected from the Taylor state (zero β), there exist some critical difference between the finite β self-organized state and the Taylor state. We now portray these points which differentiate this state from the Taylor state. As a representative parameter to manifest the difference, we focus on the Taylor constant μ, given by $\mu = (\mathbf{j} \cdot \mathbf{B})/(\mathbf{B} \cdot \mathbf{B})$. Figure 11 shows the temporal evolution of the deviation parameter $\delta\mu$ from the averaged one $< \mu >$, which is defined by

$$\delta\mu = \left\{ \frac{< (\mu - < \mu >)^2 >}{< \mu >^2} \right\}^{1/2} \tag{13}$$

for three different resistivity cases (Cases A, B and C). Since the Taylor constant μ is spatially uniform, $\delta\mu$ is expected to vanish for the Taylor's minimum energy state.[1)] Two drastic increases of $\delta\mu$ in accordance with the first and second relaxation phases indicate that the spatial structure is largey altered from the force-free one during the driven magnetic reconnection process. After the second relaxation $\delta\mu$ decreases monotonously and approaches to a small but non zero value. It should be emphasized that the value of $\delta\mu_{fin}$, or the deviation from the force-free profile, becomes more evident as the resistivity decreases.

Figure 12 shows the temporal evolutions of $< |\mathbf{j} \times \mathbf{B}|^2 >$ (solid line) and $< |\nabla p|^2 >$ (dashed line) for the same cases as Fig. 11. Two peaks appear in the evolution curves in accordance with the excitation of magnetic reconnection in the first and second relaxation phases for Cases A and B. The behavior of $< |\nabla p|^2 >$ exhibits an almost complete coincidence with that of $< |\mathbf{j} \times \mathbf{B}|^2 >$. This result ensures that the thermal pressure structure is created in such a way that the pressure-gradient force is balanced with the $\mathbf{j} \times \mathbf{B}$ force. As the quantity of $< |\mathbf{j} \times \mathbf{B}|^2 >$ is regarded as representing a deviation from the force-free profile of the magnetic field, the final state definitely deviates from the force-free one, particularly for a weaker resistivity condition. This assures that the fast process, "driven magnetic reconnection", is again a key process in the present finite

β MHD relaxation as was the case for the Taylor relaxation.

We have seen in Fig. 12 that the force-balance relation is satisfied in the relaxed state. Let us see more elaborately how the force balance relation, $\nabla p = \mathbf{j} \times \mathbf{B}$, is satisfied over the whole simulation domain. To do this we introduce a new quantity $\mathbf{B}^*$ defined by

$$\mathbf{B}^* = \mathbf{B} - (\mathbf{j} \times \mathbf{B} - \nabla p) \times \mathbf{j}/(\mathbf{j} \cdot \mathbf{j}). \tag{14}$$

We note that this quantity $\mathbf{B}^*$ becomes exactly equal to the real magnetic field $\mathbf{B}$ when the ∇p force is balanced with the $\mathbf{j} \times \mathbf{B}$ force. Figure 13 shows the vector plots of the field $\mathbf{B}^*$ and the magnetic field in the (x, y) plane (left-top and left-bottom panels) and in the (x, z) plane (right-top and right-bottom panels) at $t = 73.1 t_A$ for Case A. One can notice that the spatial profile of the field $\mathbf{B}^*$ is very similar to that of the magnetic field. In other words, the spatial profile satisfying the force-balance condition $\nabla p = \mathbf{j} \times \mathbf{B}$ over the whole simulation domain is really realized in the final stage of the energy relaxation. It is concluded therefore that in the presence of a finite thermal pressure the plasma relaxes to a state with a definite pressure structure, which is described by $\nabla p = \mathbf{j} \times \mathbf{B}$, not to the Taylor's force-free minimum energy state. The deviation from the Taylor's force-free state becomes more definite for a weaker resistivity condition.

D. Independence of the initial plasma beta

The existence of a finite thermal pressure makes the relaxed state different from the Taylor's force-free one. We here examine the dependence of the deviation from the Taylor structure on the β value of the thermal pressure. Figure 14 shows the temporal evolutions of the total magnetic energy W and the total magnetic helicity K for three cases with different initial plasma betas given in Table 1, namely, for Case B ($\beta = 0.6$), Case D ($\beta = 0.4$), Case E ($\beta = 0.2$).

As a whole, no significant difference is observed among the three cases except that the onset time of the relaxation phase is slightly delayed as β increases, though very faintly,

for the β value range of 0.2 - 0.6. For any case the selective dissipation of the magnetic energy takes place in two steps. In contrast, the total magnetic helicity decays slowly compared with the magnetic energy. It is to be noted, however, that the decay rate is in reality slowed down in two steps, when we carefully look at its decaying behavior.

Figure 15 shows the temporal envolutions of the parallel component $J_{\|}$ and the perpendicular component $J_{\perp}$ of the electric current for the same cases as Fig. 14. The perpendicular component, which is generated during the two relaxation phases, remains finite even in the final relaxed state and the amplitude is comparable to that of the parallel component regardless of the value of β for $\beta = 0.2 - 0.6$. Figure 16 shows the temporal evolution of the time scale function R(t) for the same cases as Fig. 14, which is the ratio of the time scale for the magnetic helicity dissipation τ_{MK} to the time scale for the magnetic energy dissipation τ_{ME}, where $R(t)$, τ_{ME} and τ_{MK} are defined by

$$R(t) = \frac{\tau_{MK}}{\tau_{ME}}, \tag{15}$$

$$\tau_{ME} = \frac{\int \mathbf{B} \cdot \mathbf{B} d^3\mathbf{x}}{2\eta \int \mathbf{j} \cdot \mathbf{j} d^3\mathbf{x}}, \tag{16}$$

$$\tau_{MK} = \frac{\int \mathbf{A} \cdot \mathbf{B} d^3\mathbf{x}}{2\eta \int \mathbf{j} \cdot \mathbf{B} d^3\mathbf{x}}. \tag{17}$$

One can see that all the results are essentially superimposable with an exception of a slight delay in the onset times of the first and second relaxation phases for a high initial beta plasma. Thus, it is concluded that both the behavior of the plasma during the relaxation phases and the final relaxed state are almost independent of the amount of the thermal pressure. This conclusion suggests that unless some process to pump out quickly the produced thermal energy can operate, or if the plasma is thermally insulated perpendicularly, the system will experience a non-Taylor(non-force-free) self-organization.

IV. Summary and disscusions

With a three-dimensional simulation study we have investigated the self-organization process of a finite β MHD plasma under the condition that the plasma is thermally insulated perpendicular to the magnetic field. It is confirmed that driven magnetic reconnection plays a crucial role in the self-organization process. It is driven magnetic reconnection that actuates the selective dissipation of the magnetic energy and gives rise to the inverse and normal casecades of the magnetic helicity spectrum and the magnetic energy spectrum respectively. These features are consistent with our previous simulation results[7-10].

On top of these features, the present elaborate study has revealed a new finding. The finding is that during the two-step relaxation process subject to driven reconnection the decay rate of the magnetic helicity is critically slowed down. This implies that the helicity conservation is not a substantiated property for the MHD self-organization, though it has been widely believed so far.

It is also found that the onset time of driven magnetic reconnection is almost independent of the electrical resistivity. For a large electrical resistivity case, however, magnetic reconnection is obscure because most of the free magnetic energy dissipates before the first magnetic reconnection takes place and the process becomes almost diffusive. This indicates that a "weak electrical resistivity" condition, or a collisionless condition, is necessary for a clear-cut self-organization to take place.

We have demonstrated that a finite β MHD plasma system relaxes toward a state with a minimum magnetic energy which is similar to the pressureless case. This is because the most important physical process in self-organization is the driven magnetic reconnection process and the pressure is not the primary cause of reconnection. However, the magnetic field configuration is not described by the Taylor's force-free minimum energy state. The driven magnetic reconnection process produces an extremely heated plasma in the vicinity

of the reconnection point. The locally heated plasma modifies the magnetic field. As a result of the produced pressure gradient, the perpendicular electric current is generated to balance the pressure force. It is confirmed that the new self-organized state of a finite pressure MHD plasma is an MHD equilibrium $\mathbf{j} \times \mathbf{B} = \nabla p$, instead of the Taylor's minimum energy state where $\mathbf{j}_{\parallel} = \mu \mathbf{B}$ with a spatially uniform μ. We have also confirmed that there is no significant effect of the initial plasma β on this conclusion. This suggests that as far as the thermal energy produced by the relaxation process is confined within the system where no fast thermal conduction exists, the MHD plasma does not obey the Taylor relaxation, but experiences a non-Taylor process which leads to the force-balanced minimum energy state.

Acknowledgements

This work is perfomed by using the Advanced Computing System for Complexity Simulation at NIFS under the support of two Grants-in-Aid from the Japanese Ministry of Education, Science and Culture (No.05836038 and No.06044238). One of the authors(Zhu) would like to thank Professor X.T.He for his continuous encouragement. He is supported by the Japanese Ministry of Education, Science and Culture(MONBUSHO).

References

[1] J.B.Taylor, Phys.Rev.Lett. **33**, 1139(1974)

[2] J.B.Taylor, Rev.Mod.Phys. **58**, 741(1986),and references therein.

[3] W.H.Mattheus and D.C.Montgomery, Ann.N.Y. Acad.Sci. **357**, 203(1980).

[4] W.H.Mattheus, M.L.Goldstein and D.C.Montgomery,Phys.Rev.Lett.**51**, 1484(1983).

[5] A.Y.Aydemir and D.C.Barnes, Phys.Rev.Lett. **52**, 930(1984).

[6] R.Horiuchi and T.Sato, Phys.Rev.Lett.**55**, 211(1985).

[7] R.Horiuchi and T.Sato, Phys. Fluids **29**, 1161(1986).

[8] R.Horiuchi and T.Sato, Phys. Fluids **29**, 4174(1986).

[9] R.Horiuchi and T.Sato, Phys. Fluids **33**, 1142(1988).

[10] S.Ortolani and D.D.Schnack, Magnetohydrodynamics of plasma relaxation (World Scientific Publishing, Singapore, 1993)

[11] A.Bhattacharjee and R.L.Dewar, Phys.Fluids **25**, 887(1982).

[12] J.W.Edenstrasser and W.Schuurman, Phys. Fluids **26**, 500(1983).

[13] Y.Kondoh, Y.Hosaka, J.L.Liang, R.Horiuchi and T.Sato, J.Phys.Soc.Japan **63**, 546(1994).

[14] R.Horiuchi and T.Sato, Phys. Fluids B **1**, 581(1989).

[15] A.Reiman, Phys.Fluids **23**, 230(1980).

[16] T.Sato and T.Hayashi, Phys.Fluids **22**, 1189(1979); T.Sato, T.Hayashi, K.Watanabe, R. Horiuchi, M. Tanaka, N. Sawairi and K.Kusano, Phys.Fluids B **4**, 450(1992).

[17] T.Sato and K.Kusano, Phys.Rev.Lett. **54**, 808(1985).

[18] T.Sato, R.Horiuchi and K.Kusano, Phys.Fluids B **1** , 255(1989).

Table 1. Simulation parameters

Case	α	β	η
A	58.3	0.6	10^{-4}
B	58.3	0.6	2×10^{-4}
C	58.3	0.6	5×10^{-4}
D	58.3	0.4	2×10^{-4}
E	58.3	0.2	2×10^{-4}

Figure Captions

Fig.1: The vector plots of the poloidal magnetic field (right) and the contour plots of the toroidal magnetic field (left) in a poloidal plane (x, y) at t=0 where a contour with a negative toroidal field is plotted by a dotted line.

Fig.2: The temporal evolutions of the total magnetic energy W (solid line) and the total magnetic helicity K (dotted line) for case A where both the energy and the helicity are normalized by their initial values.

Fig.3: The temporal evolutions of the average wavenumber of the energy spectrum (solid line) and that of the helicity spectrum (dotted line) as the same case with Fig.2.

Fig.4: The temporal evolutions of the total energy dissipation D_W and the total helicity dissipation D_K as the same case with Fig.2, where $D_W = \int (\mathbf{j} \cdot \mathbf{j}) d^3\mathbf{x}$ and $D_K = \int (\mathbf{j} \cdot \mathbf{B}) d^3\mathbf{x}$.

Fig.5: The vector plots of the poloidal velocity (v_x, v_y) (top-left), the contour maps of the toroidal magnetic filed B_z (top-right), the toroidal electric current j_z (bottom-left) and the pressure p (bottom-right) in the poloidal cross-section ($z = L_z/2$) at $t = 18t_A$ for Case A where a contour with a negative value of B_z or j_z and a contour less than the average value of p are plotted by a dotted line.

Fig.6: The bird's-eye views of the profiles for $\mathbf{j} \cdot \mathbf{j}$ (top) and $-\mathbf{j} \cdot \mathbf{B}$ (bottom) in the poloidal cross-section ($z = L_z/2$) at $t = 20.43t_A$ for Case A, where only the negative part of $\mathbf{j} \cdot \mathbf{B}$ is displayed in the bottom panel.

Fig.7: The contour maps of the toroidal magnetic field (top), and the pressure (bottom) at $t = 19.0t_A$ (left), $t = 32.4t_A$ (middle), and $t = 71.3t_A$ (right) for Case C where the red color stands for a contour larger than the average value of p or the positive toroidal magnetic field.

Fig.8: The temporal evolution of the average pressure fluctuation δp.

Fig.9: The temporal envolutions of the normalized parallel component $J_{\|}$ and the normalized perpendicular component $J_{\perp}$ of the electric current for Case A (solid line), Case B (dashed line), Case C(dot-dashed line), where $J_{\|} =< |\mathbf{j}_{\|}|/|\mathbf{j}| >$ and $J_{\perp} =< |\mathbf{j}_{\perp}|/|\mathbf{j}| >$.

Fig.10: A three-dimensional display of the isosurfaces of the toroidal magnetic field and the pressure at $t = 0$, $t = 19.0t_A$, $t = 32.4t_A$, and $t = 71.3t_A$ for Case C.

Fig.11: The temporal evolutions of $\delta\mu$ for Case A (solid line), Case B (dashed line) and Case C (dot-dashed line), where $\delta\mu$ is defined by Eq.(13).

Fig.12: The temporal evolutions of $< |\nabla p|^2 >$ (dashed line) and $< |\mathbf{j} \times \mathbf{B}|^2 >$ (solid line) for the same cases as Figure 11.

Fig.13: The vector plots of the field $\mathbf{B}^*$ and the magnetic field in an (x, y) plane (left-top and left-bottom panels) and in the (x, z) plane (right-top and right-bottom panels) at $t = 73.1t_A$ for Case A, where $\mathbf{B}^*$ is defined by Eq.14.

Fig.14: The temporal evolutions of the total magnetic energy W and the total

magnetic helicity K for three cases with different initial plasma betas where both the energy and the helicity are normalized by their initial values, and the solid, dashed and dot-dashed lines correspond to those for Case B ($\beta = 0.6$), Case D ($\beta = 0.4$), Case E ($\beta = 0.2$), respectively.

Fig.15: The temporal envolutions of the normalized parallel component $J_{\|}$ and the normalized perpendicular component $J_{\perp}$ of the electric current for the same cases as Fig. 14.

Fig.16: The temporal evolutions of the function R(t) for the same cases as Fig. 14, where R(t) is the ratio of the time scale for the magnetic helicity dissipation to the time scale for the magnetic energy dissipation.

Fig.1

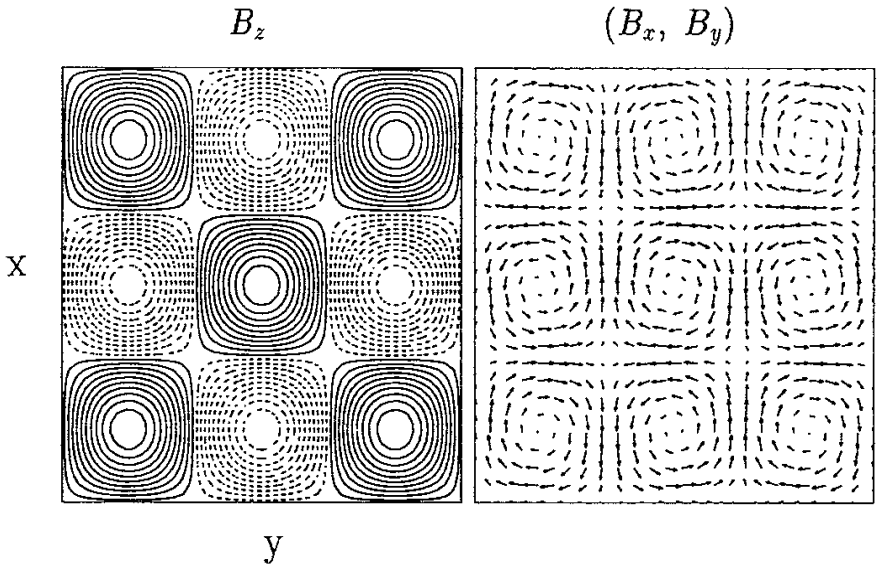

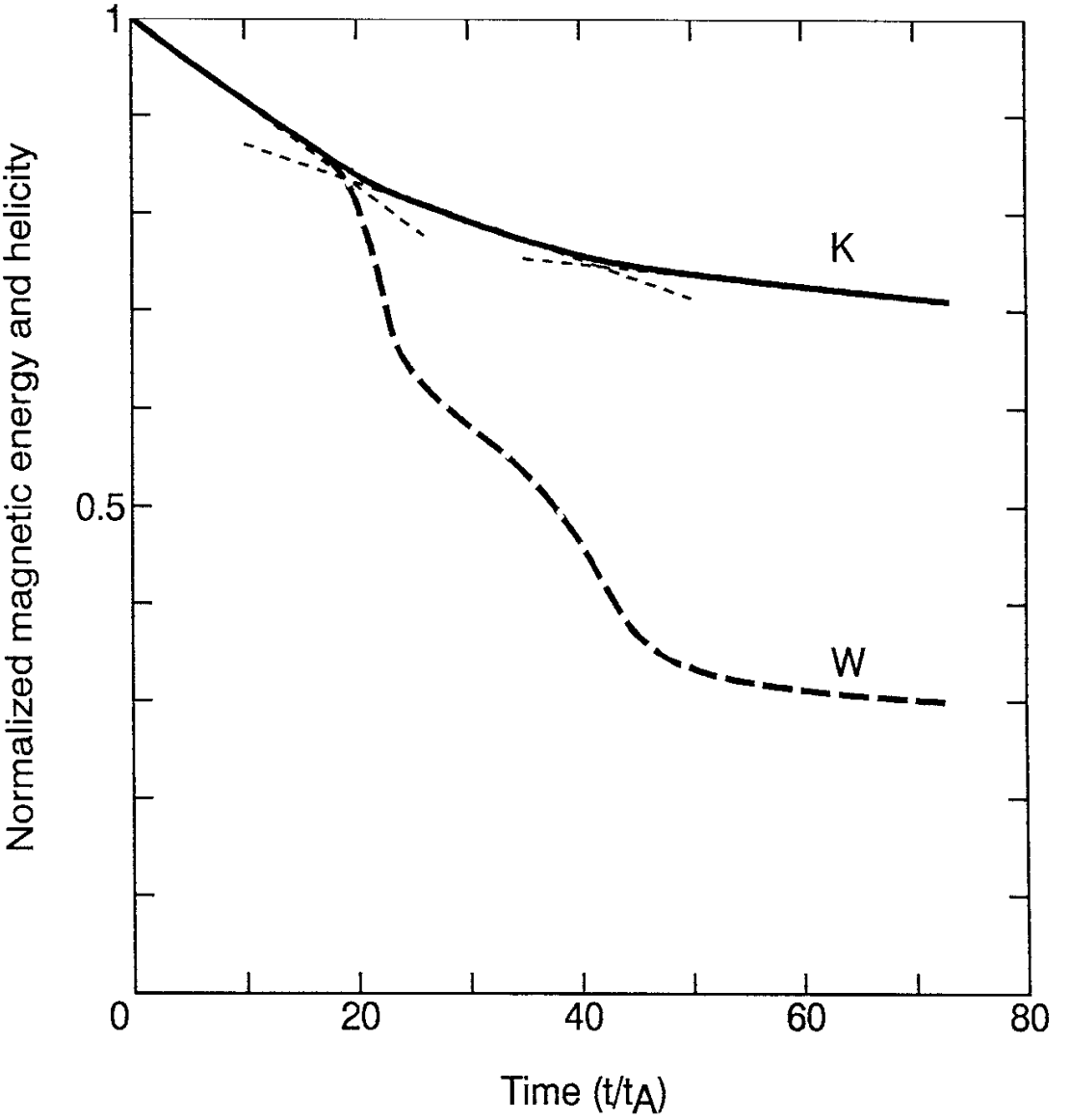

Fig.2 (Zhu, Horiuchi and Sato)

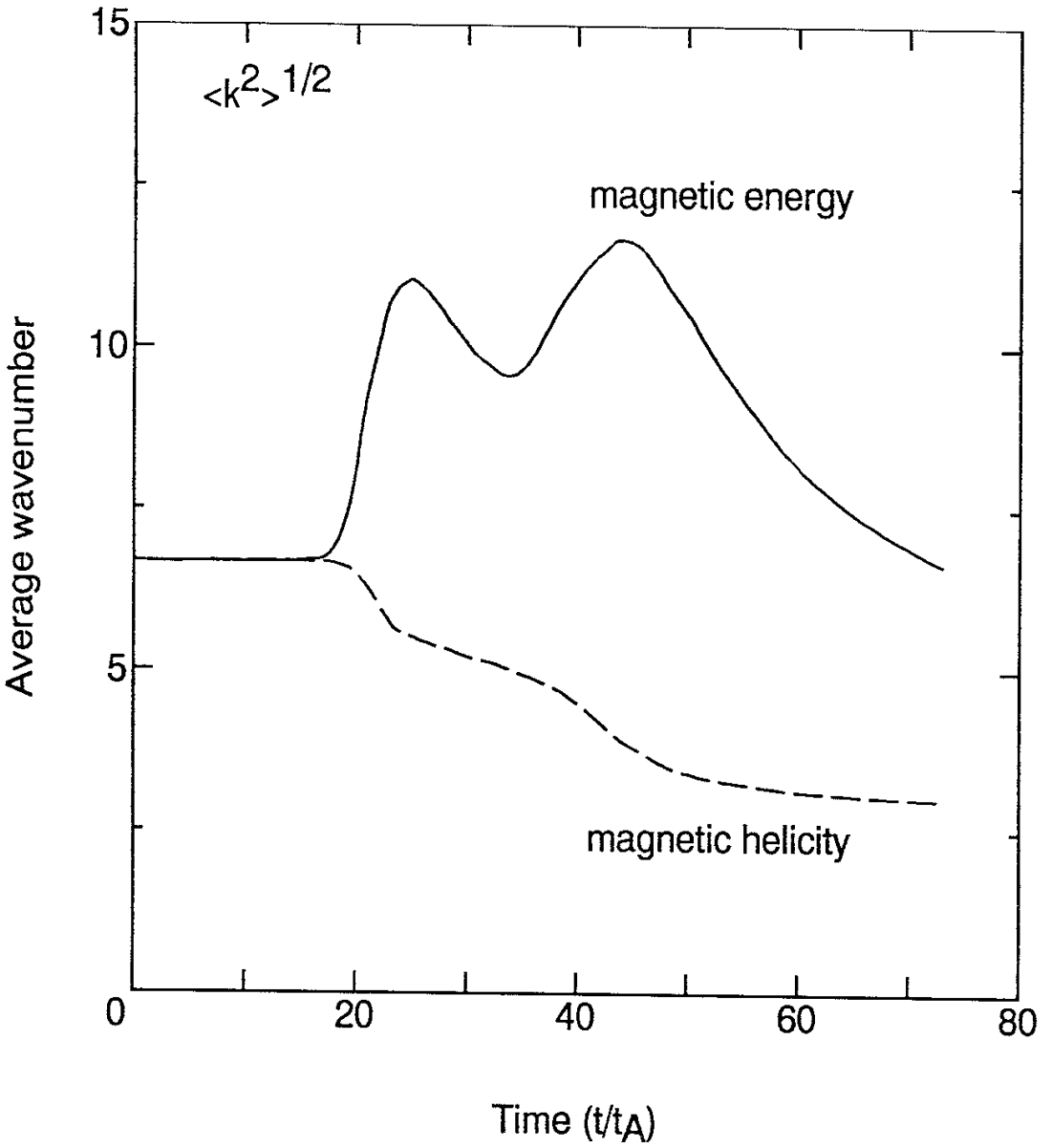

Fig.3 (Zhu, Horiuchi and Sato)

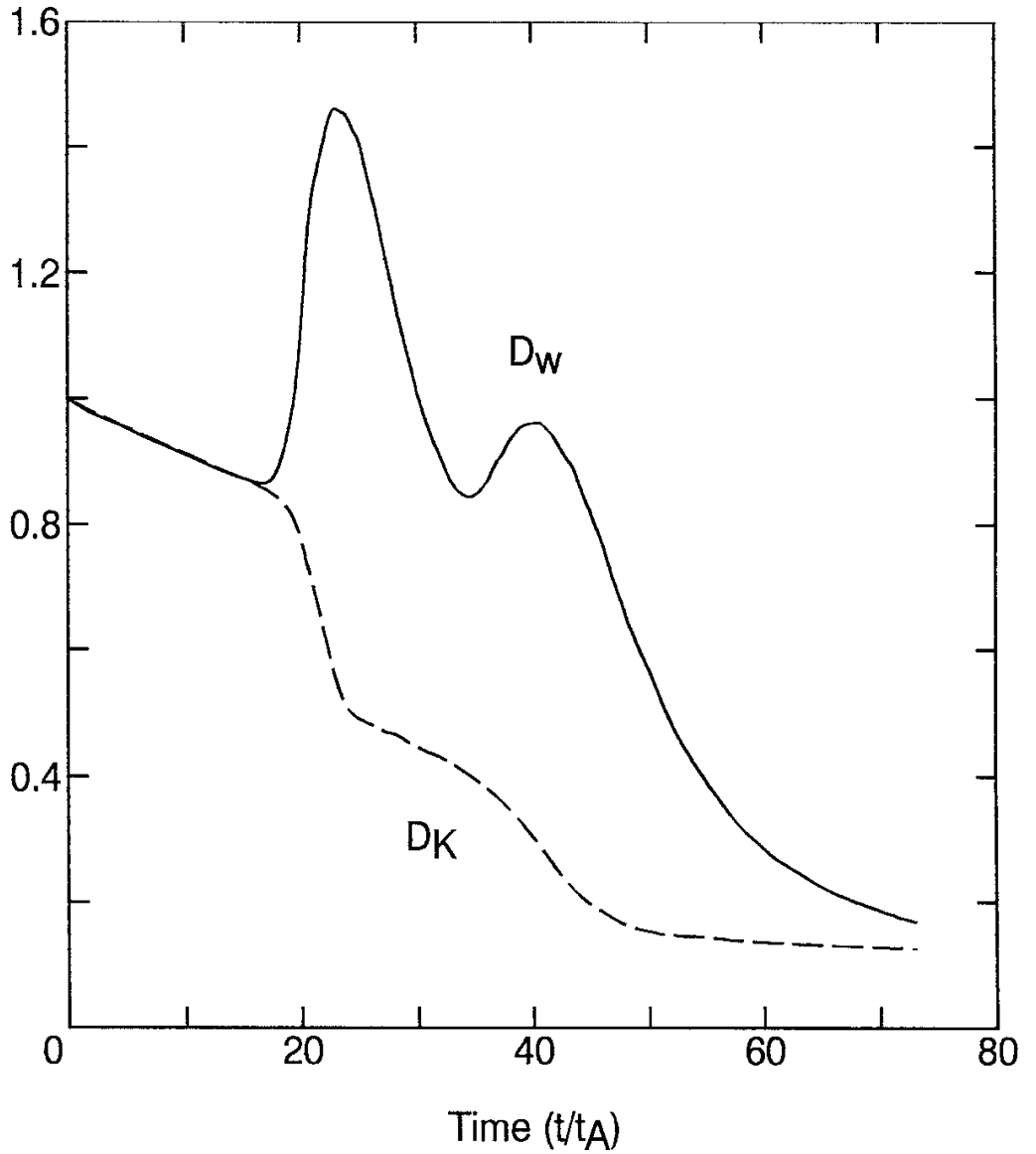

Fig.4 (Zhu, Horiuchi and Sato)

Fig.5 (Zhu, Horiuchi and Sato)

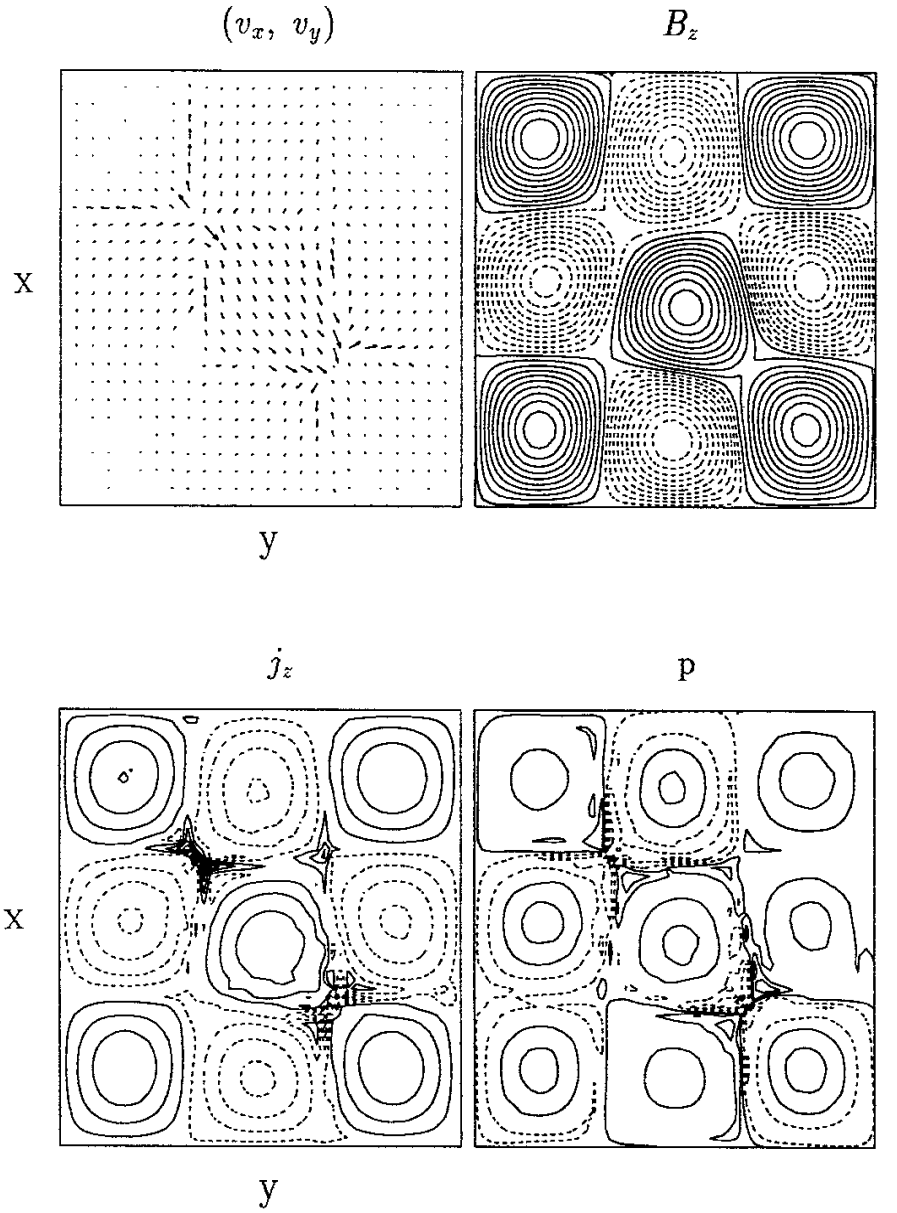

Fig.6

$j \cdot j$

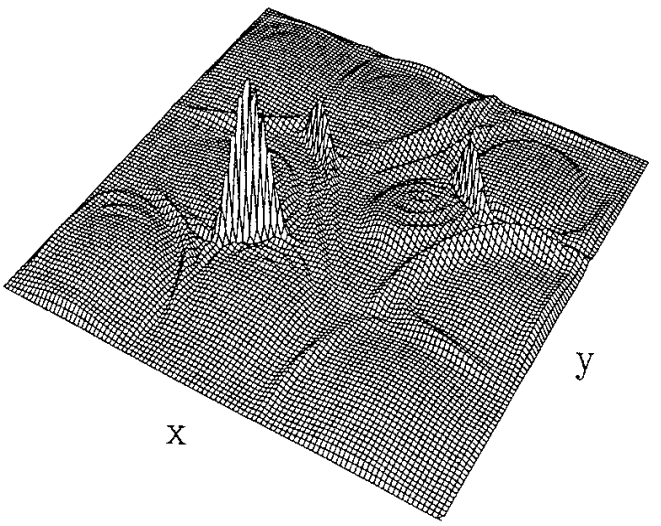

$-j \cdot B$

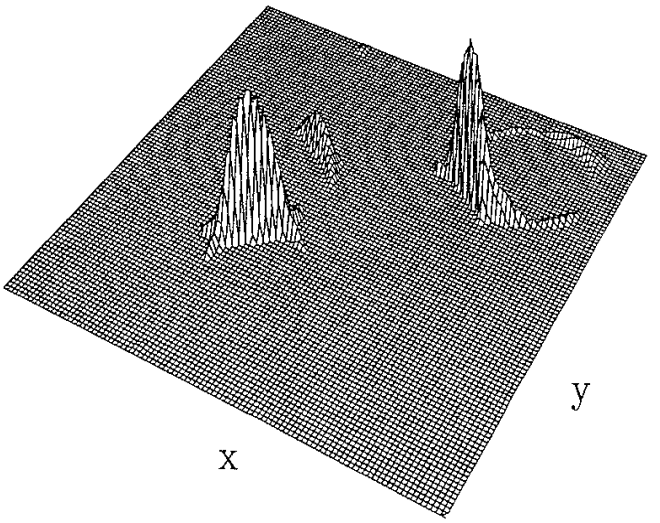

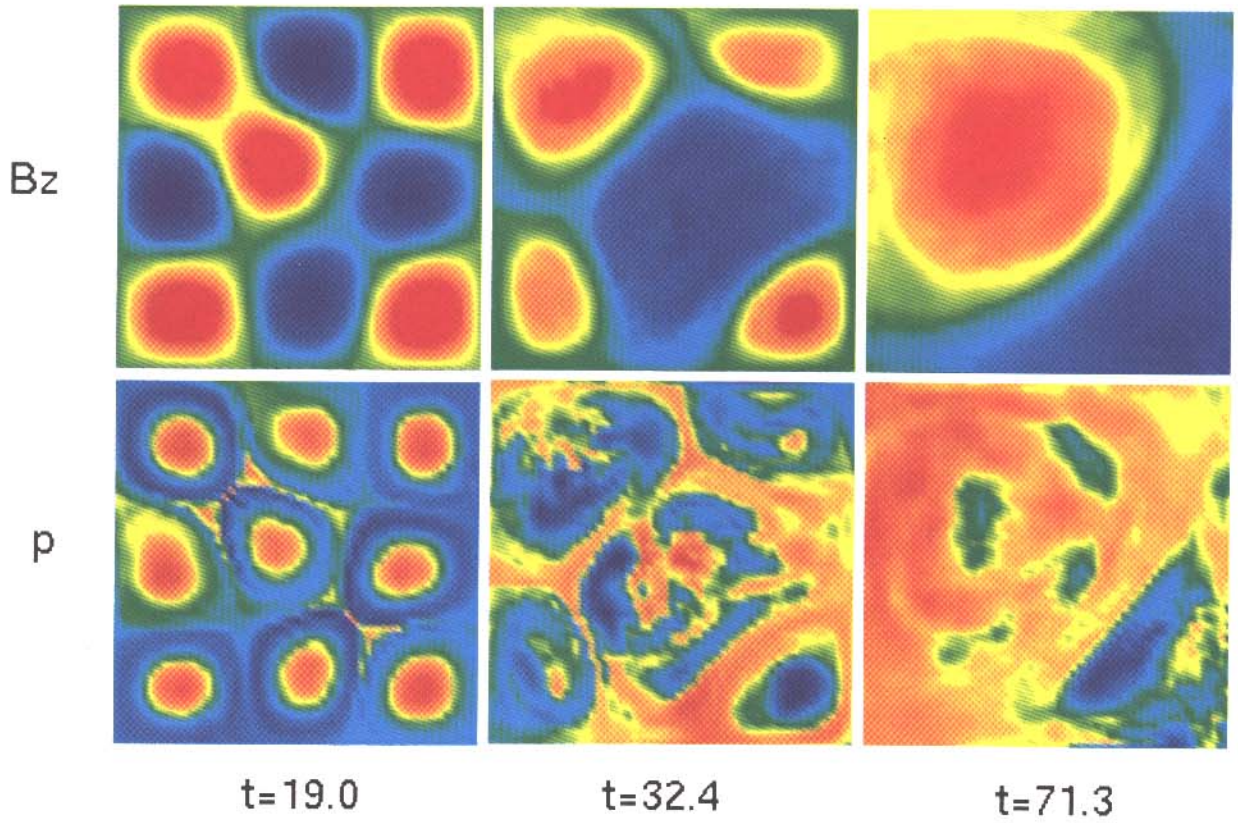

Fig.7 (Zhu, Horiuchi and Sato)

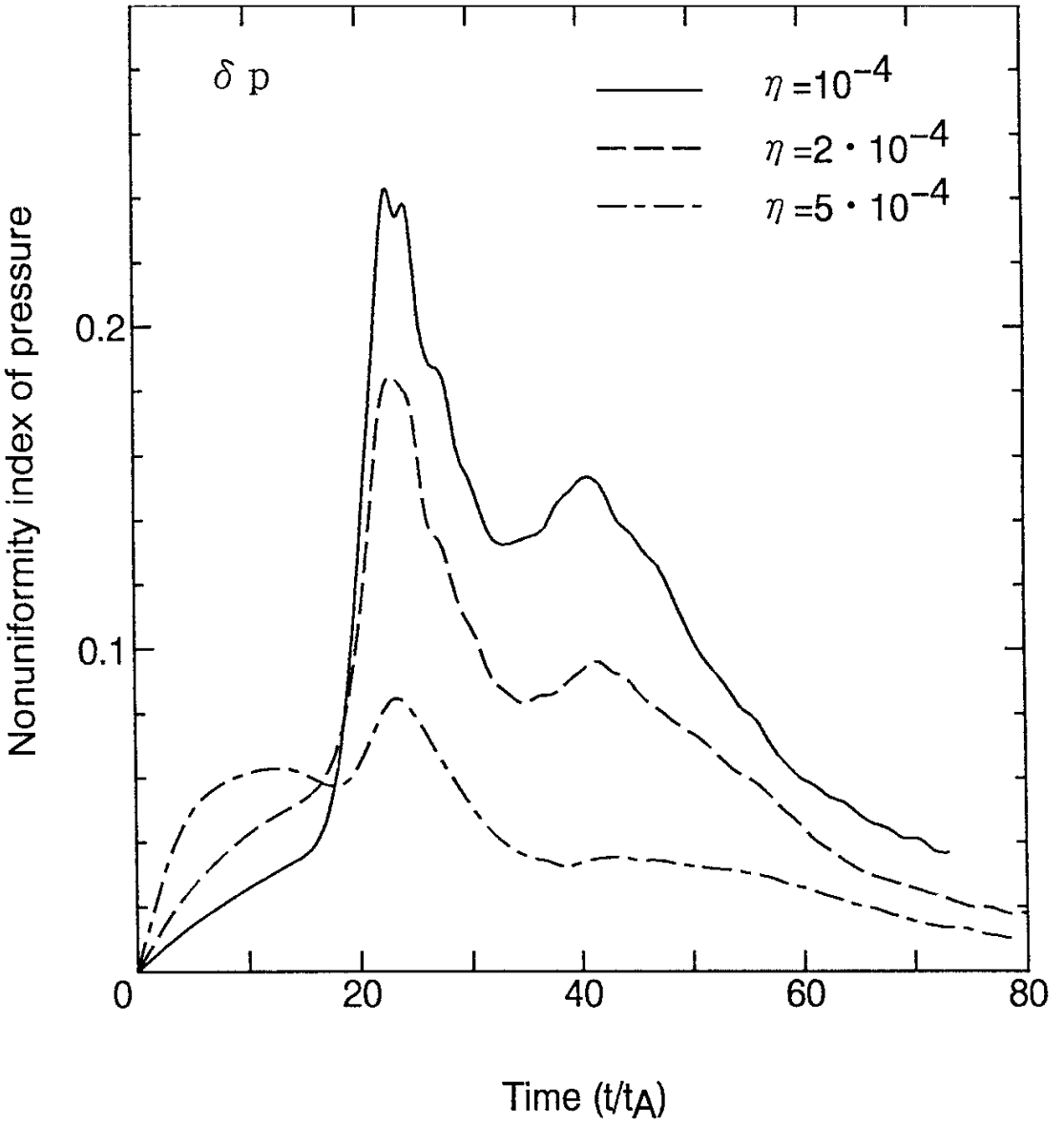

Fig.8 (Zhu, Horiuchi and Sato)

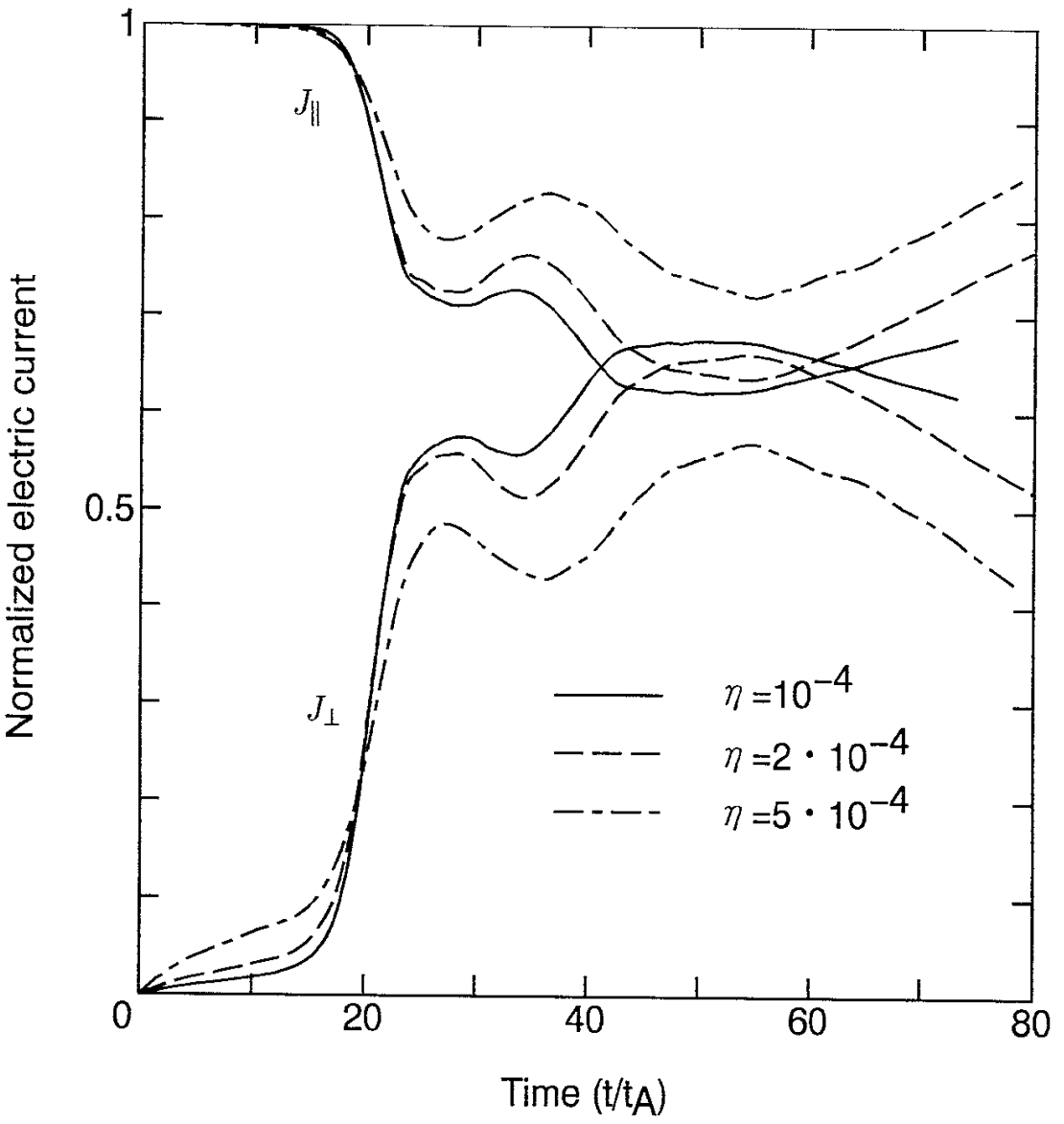

Fig.9 (Zhu, Horiuchi and Sato)

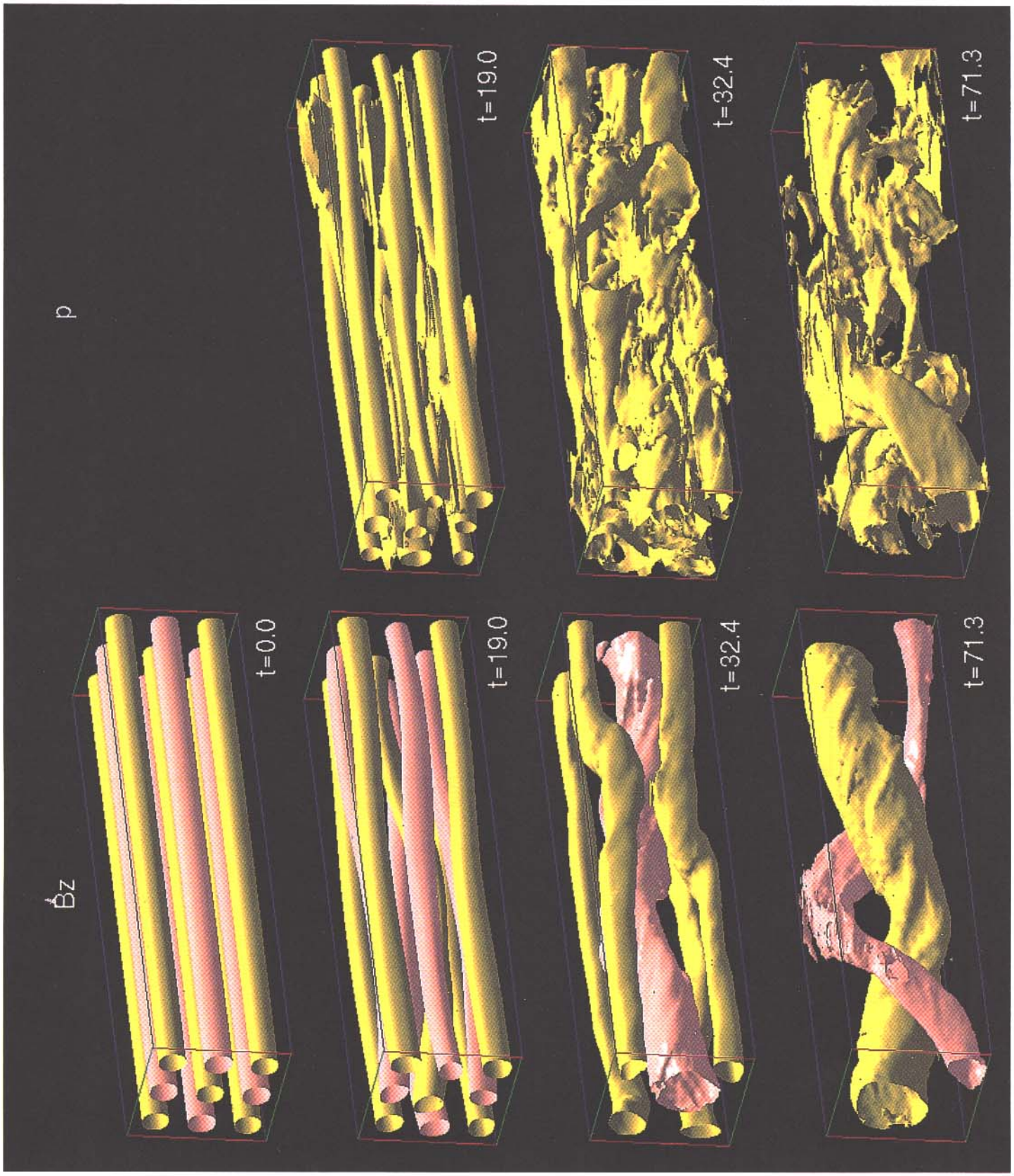

Fig.10 (Zhu, Horiuchi and Sato)

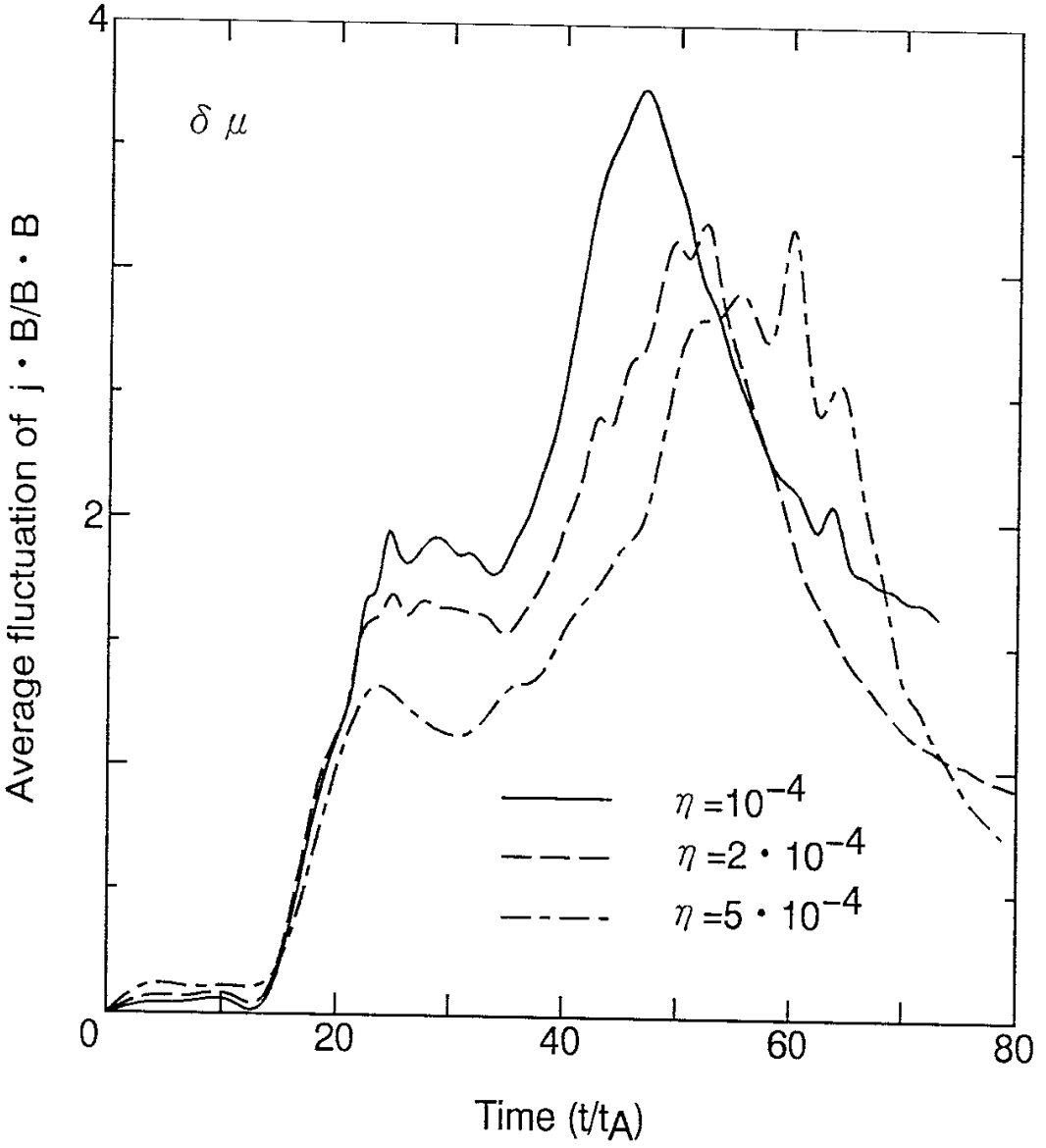

Fig.11 (Zhu,Horiuchi and Sato)

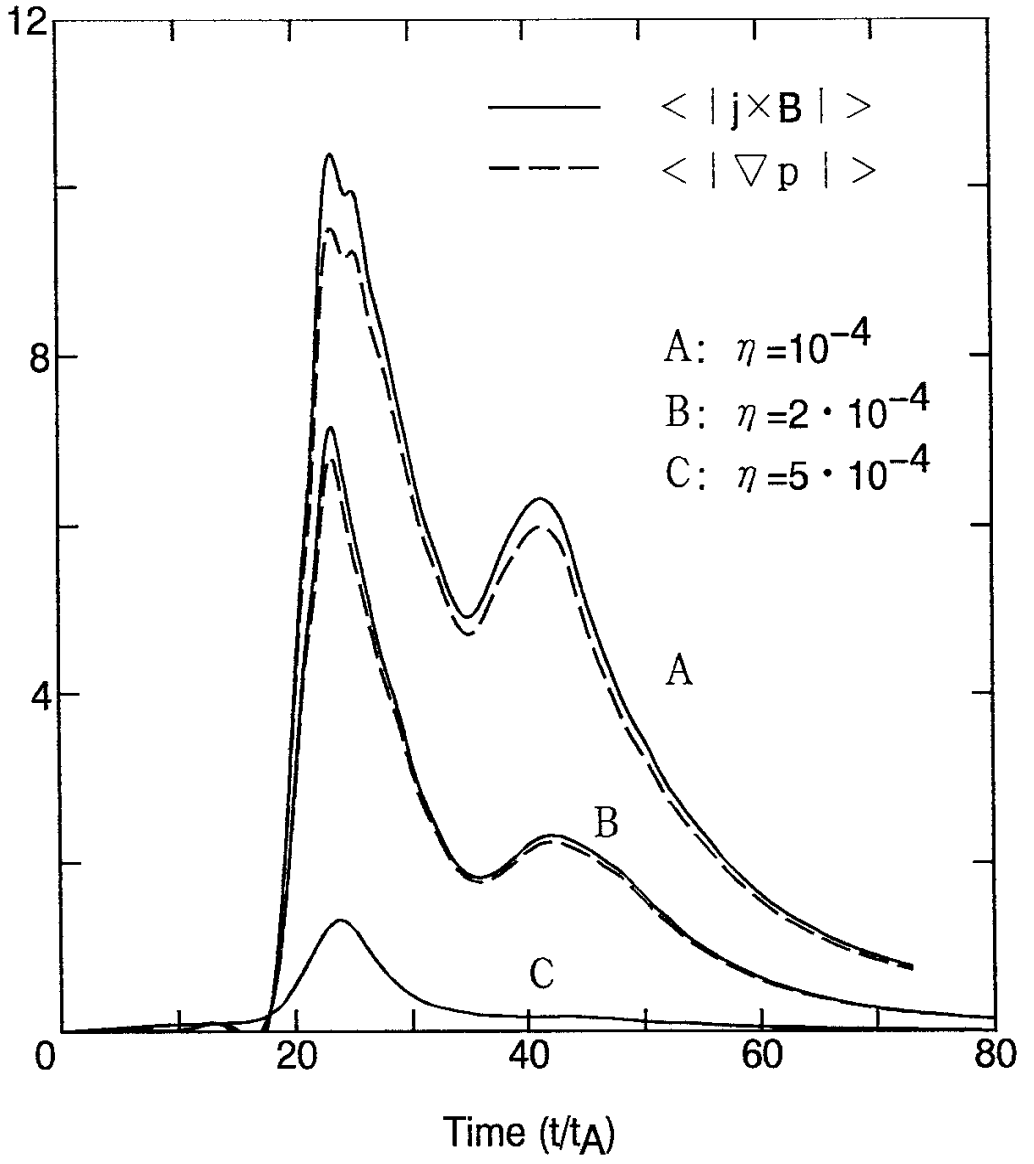

Fig.12 (Zhu,Horiuchi and Sato)

Fig.13 (Zhu, Horiuchi and Sato)

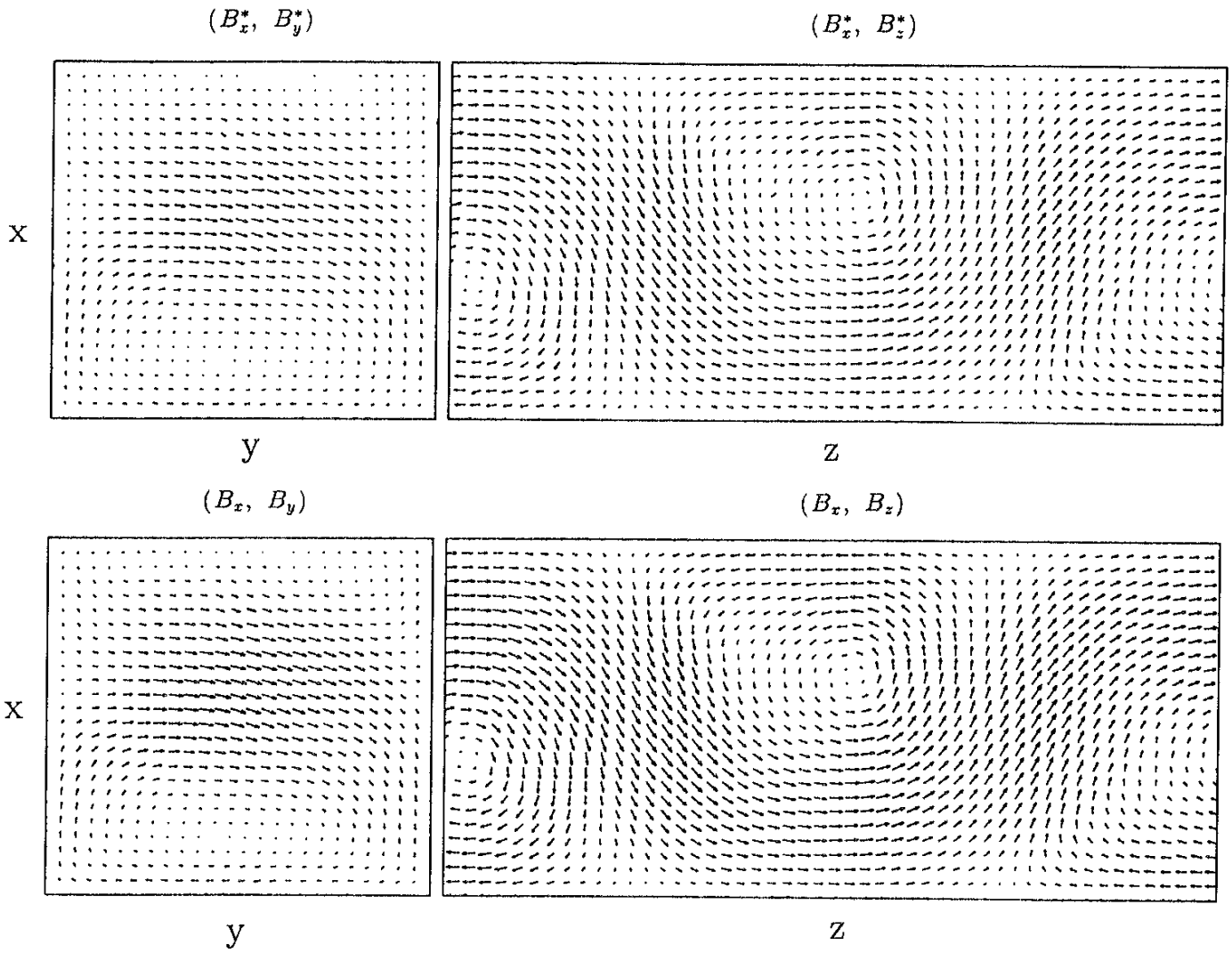

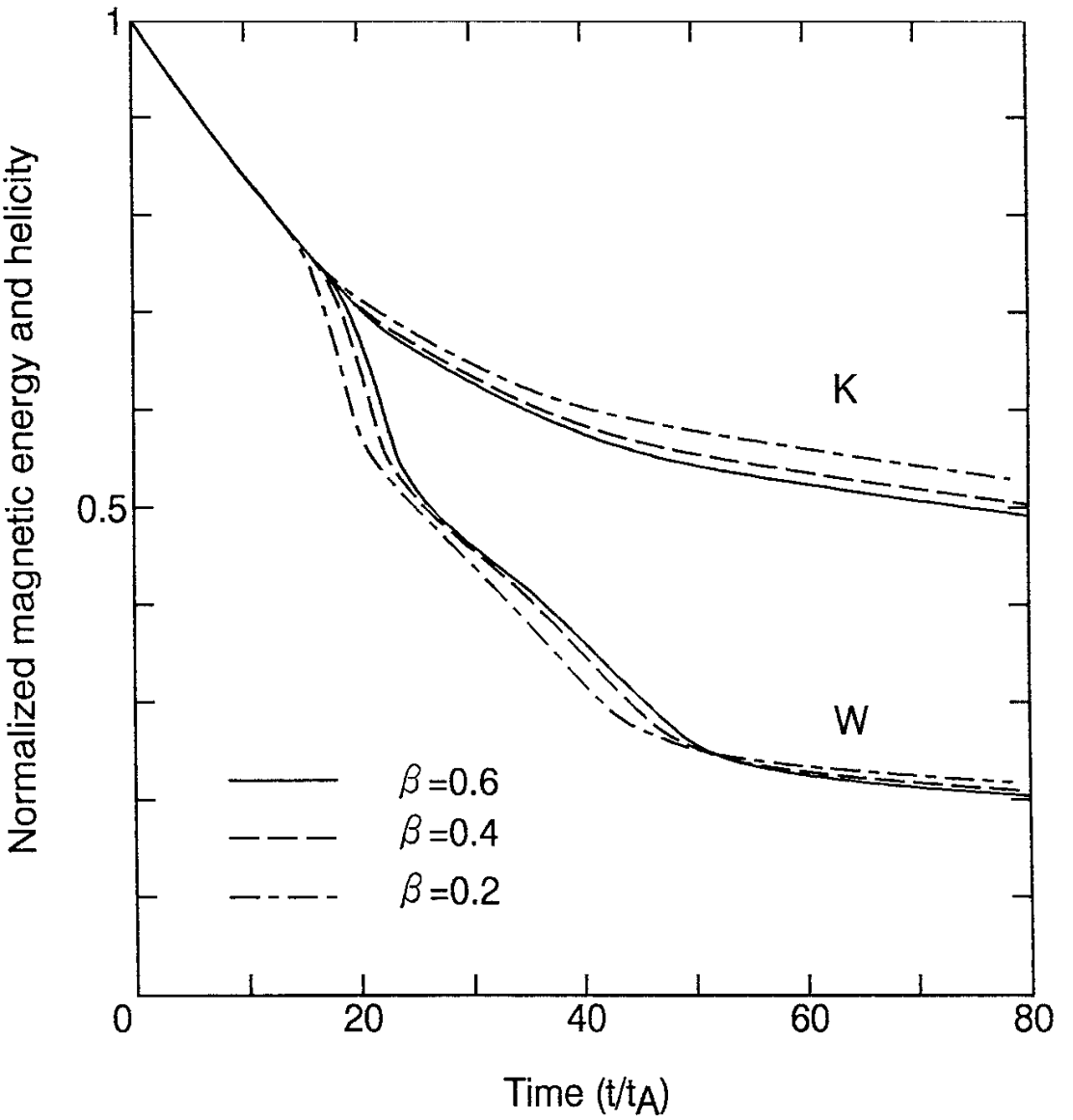

Fig.14 (Zhu, Horiuchi and Sato)

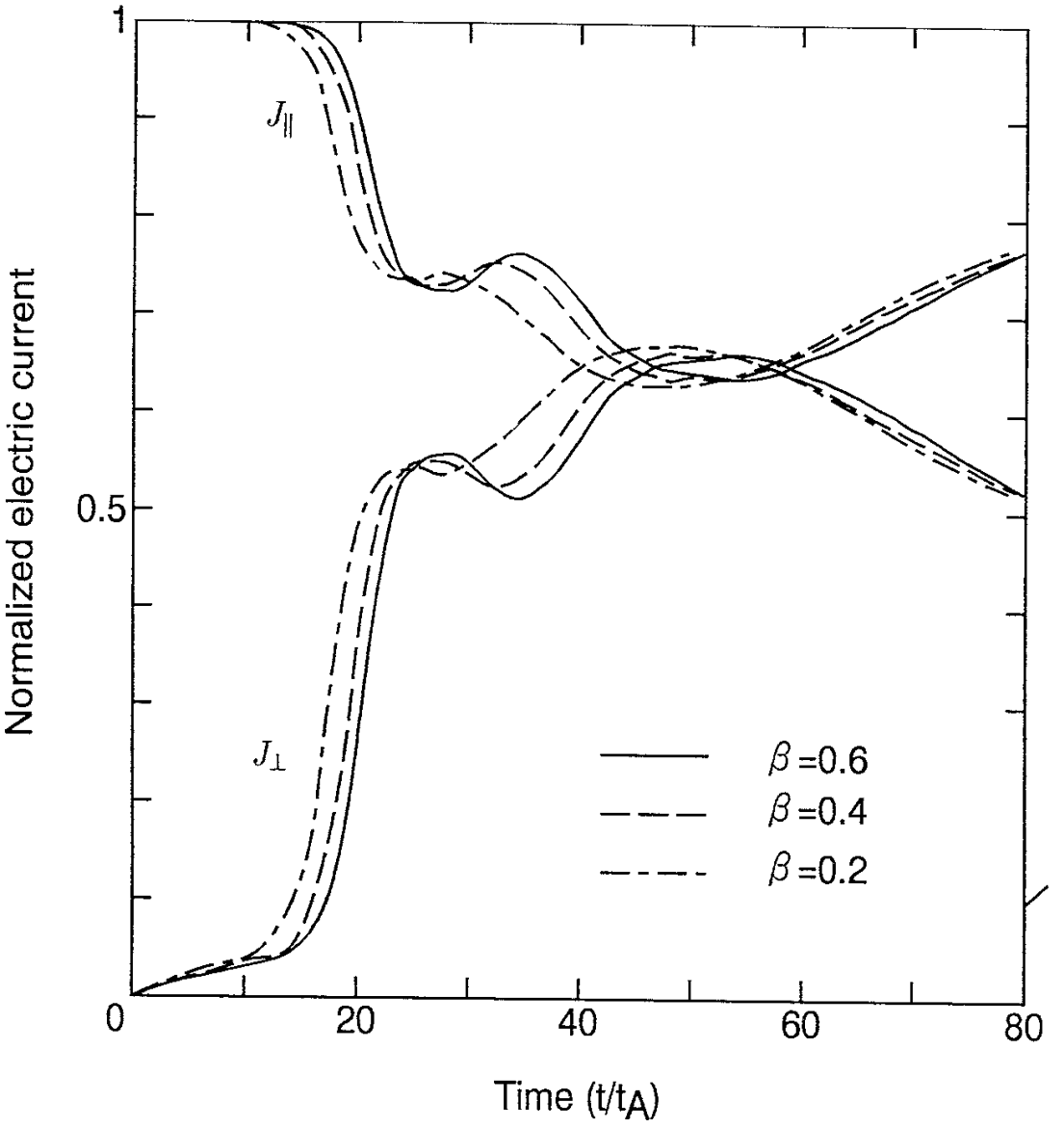

Fig.15 (Zhu,Horiuchi and Sato)

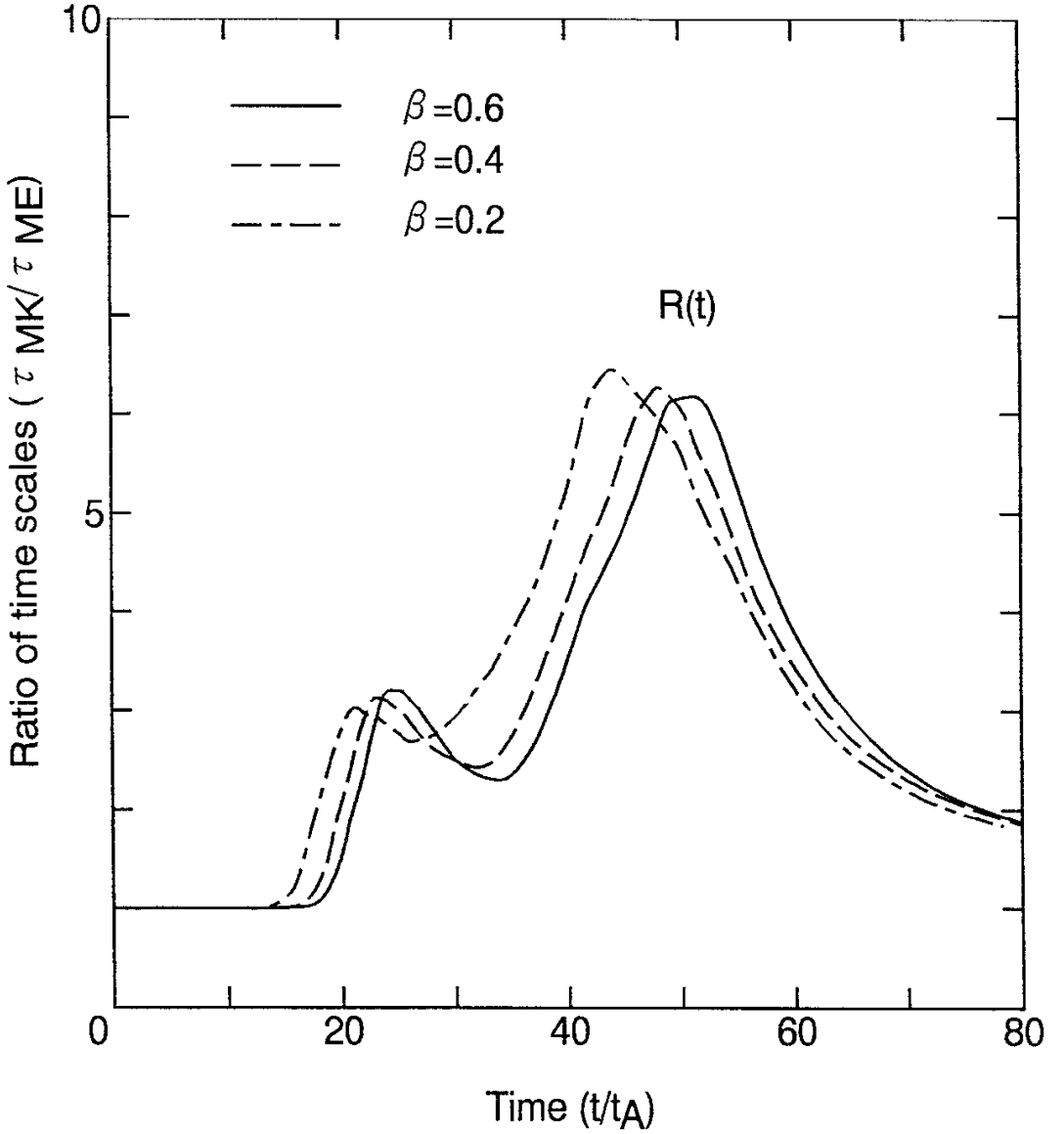

Fig.16 (Zhu,Horiuchi and Sato)

Recent Issues of NIFS Series

NIFS-276 R.V. Reddy, K. Watanabe, T. Sato and T.H. Watanabe,
Impulsive Alfven Coupling between the Magnetosphere and Ionosphere;
Apr.1994

NIFS-277 J. Uramoto,
A Possibility of π^- Meson Production by a Low Energy Electron Bunch and Positive Ion Bunch; Apr. 1994

NIFS-278 K. Itoh, S.-I. Itoh, A. Fukuyama, M. Yagi and M. Azumi,
Self-sustained Turbulence and L-mode Confinement in Toroidal Plasmas II; Apr. 1994

NIFS-279 K. Yamazaki and K.Y.Watanabe,
New Modular Heliotron System Compatible with Closed Helical Divertor and Good Plasma Confinement; Apr. 1994

NIFS-280 S. Okamura, K. Matsuoka, K. Nishimura, K. Tsumori, R. Akiyama, S. Sakakibara, H. Yamada, S. Morita, T. Morisaki,. N. Nakajima, K. Tanaka, J. Xu, K. Ida, H. Iguchi, A. Lazaros, T. Ozaki, H. Arimoto, A. Ejiri, M. Fujiwara, H. Idei. O. Kaneko, K. Kawahata, T. Kawamoto, A. Komori, S. Kubo, O. Motojima, V.D. Pustovitov, C. Takahashi, K. Toi and I. Yamada,
High-Beta Discharges with Neutral Beam Injection in CHS; Apr. 1994

NIFS-281 K. Kamada, H. Kinoshita and H. Takahashi,
Anomalous Heat Evolution of Deuteron Implanted Al on Electron Bombardment ; May 1994

NIFS-282 H. Takamaru, T. Sato, K. Watanabe and R. Horiuchi,
Super Ion Acoustic Double Layer; May 1994

NIFS-283 O.Mitarai and S. Sudo
Ignition Characteristics in D-T Helical Reactors; June 1994

NIFS-284 R. Horiuchi and T. Sato,
Particle Simulation Study of Driven Magnetic Reconnection in a Collisionless Plasma; June 1994

NIFS-285 K.Y. Watanabe, N. Nakajima, M. Okamoto, K. Yamazaki, Y. Nakamura, M. Wakatani,
Effect of Collisionality and Radial Electric Field on Bootstrap Current in LHD (Large Helical Device); June 1994

NIFS-286 H. Sanuki, K. Itoh, J. Todoroki, K. Ida, H. Idei, H. Iguchi and H. Yamada,
Theoretical and Experimental Studies on Electric Field and Confinement in Helical Systems; June 1994

NIFS-287 K. Itoh and S-I. Itoh,
Influence of the Wall Material on the H-mode Performance; June 1994

NIFS-288 K. Itoh, A. Fukuyama, S.-I. Itoh, M. Yagi and M. Azumi
Self-Sustained Magnetic Braiding in Toroidal Plasmas: July 1994

NIFS-289 Y. Nejoh,
Relativistic Effects on Large Amplitude Nonlinear Langmuir Waves in a Two-Fluid Plasma; July 1994

NIFS-290 N. Ohyabu, A. Komori, K. Akaishi, N. Inoue, Y. Kubota, A.I. Livshit, N. Noda, A. Sagara, H. Suzuki, T. Watanabe, O. Motojima, M. Fujiwara, A. Iiyoshi,
Innovative Divertor Concepts for LHD; July 1994

NIFS-291 H. Idei, K. Ida, H. Sanuki, S. Kubo, H. Yamada, H. Iguchi, S. Morita, S. Okamura, R. Akiyama, H. Arimoto, K. Matsuoka, K. Nishimura, K. Ohkubo, C. Takahashi, Y. Takita, K. Toi, K. Tsumori and I. Yamada,
Formation of Positive Radial Electric Field by Electron Cyclotron Heating in Compact Helical System; July 1994

NIFS-292 N. Noda, A. Sagara, H. Yamada, Y. Kubota, N. Inoue, K. Akaishi, O. Motojima, K. Iwamoto, M. Hashiba, I. Fujita, T. Hino, T. Yamashina, K. Okazaki, J. Rice, M. Yamage, H. Toyoda and H. Sugai,
Boronization Study for Application to Large Helical Device; July 1994

NIFS-293 Y. Ueda, T. Tanabe, V. Philipps, L. Könen, A. Pospieszczyk, U. Samm, B. Schweer, B. Unterberg, M. Wada, N. Hawkes and N. Noda,
Effects of Impurities Released from High Z Test Limiter on Plasma Performance in TEXTOR; July. 1994

NIFS-294 K. Akaishi, Y. Kubota, K. Ezaki and O. Motojima,
Experimental Study on Scaling Law of Outgassing Rate with A Pumping Parameter, Aug. 1994

NIFS-295 S. Bazdenkov, T. Sato, R. Horiuchi, K. Watanabe
Magnetic Mirror Effect as a Trigger of Collisionless Magnetic Reconnection, Aug. 1994

NIFS-296 K. Itoh, M. Yagi, S.-I. Itoh, A. Fukuyama, H. Sanuki, M. Azumi
Anomalous Transport Theory for Toroidal Helical Plasmas,
Aug. 1994 (IAEA-CN-60/D-III-3)

NIFS-297 J. Yamamoto, O. Motojima, T. Mito, K. Takahata, N. Yanagi, S. Yamada, H. Chikaraishi, S. Imagawa, A. Iwamoto, H. Kaneko, A. Nishimura, S. Satoh, T. Satow, H. Tamura, S. Yamaguchi, K. Yamazaki, M. Fujiwara, A. Iiyoshi and LHD group,

New Evaluation Method of Superconductor Characteristics for Realizing the Large Helical Device; Aug. 1994 (IAEA-CN-60/F-P-3)

NIFS-298 A. Komori, N. Ohyabu, T. Watanabe, H. Suzuki, A. Sagara, N. Noda, K. Akaishi, N. Inoue, Y. Kubota, O Motojima, M. Fujiwara and A. Iiyoshi, *Local Island Divertor Concept for LHD*; Aug. 1994 (IAEA-CN-60/F-P-4)

NIFS-299 K. Toi, T. Morisaki, S. Sakakibara, A. Ejiri, H. Yamada, S. Morita, K. Tanaka, N. Nakajima, S. Okamura, H. Iguchi, K. Ida, K. Tsumori, S. Ohdachi, K. Nishimura, K. Matsuoka, J. Xu, I. Yamada, T. Minami, K. Narihara, R. Akiyama, A. Ando, H. Arimoto, A. Fujisawa, M. Fujiwara, H. Idei, O. Kaneko, K. Kawahata, A. Komori, S. Kubo, R. Kumazawa, T. Ozaki, A. Sagara, C. Takahashi, Y. Takita and T. Watari
Impact of Rotational-Transform Profile Control on Plasma Confinement and Stability in CHS; Aug. 1994 (IAEA-CN-60/A6/C-P-3)

NIFS-300 H. Sugama and W. Horton,
Dynamical Model of Pressure-Gradient-Driven Turbulence and Shear Flow Generation in L-H Transition; Aug. 1994 (IAEA/CN-60/D-P-I-11)

NIFS-301 Y. Hamada, A. Nishizawa, Y. Kawasumi, K.N. Sato, H. Sakakita, R. Liang, K. Kawahata, A. Ejiri, K. Narihara, K. Sato, T. Seki, K. Toi, K. Itoh, H. Iguchi, A. Fujisawa, K. Adachi, S. Hidekuma, S. Hirokura, K. Ida, M. Kojima, J. Koog, R. Kumazawa, H. Kuramoto, T. Minami, I. Negi, S. Ohdachi, M. Sasao, T. Tsuzuki, J. Xu, I. Yamada, T. Watari,
Study of Turbulence and Plasma Potential in JIPP T-IIU Tokamak;
Aug. 1994 (IAEA/CN-60/A-2-III-5)

NIFS-302 K. Nishimura, R. Kumazawa, T. Mutoh, T. Watari, T. Seki, A. Ando, S. Masuda, F. Shinpo, S. Murakami, S. Okamura, H. Yamada, K. Matsuoka, S. Morita, T. Ozaki, K. Ida, H. Iguchi, I. Yamada, A. Ejiri, H. Idei, S. Muto, K. Tanaka, J. Xu, R. Akiyama, H. Arimoto, M. Isobe, M. Iwase, O. Kaneko, S. Kubo, T. Kawamoto, A. Lazaros, T. Morisaki, S. Sakakibara, Y. Takita, C. Takahashi and K. Tsumori,
ICRF Heating in CHS; Sep. 1994 (IAEA-CN-60/A-6-I-4)

NIFS-303 S. Okamura, K. Matsuoka, K. Nishimura, K. Tsumori, R. Akiyama, S. Sakakibara, H. Yamada, S. Morita, T. Morisaki, N. Nakajima, K. Tanaka, J. Xu, K. Ida, H. Iguchi, A. Lazaros, T. Ozaki, H. Arimoto, A. Ejiri, M. Fujiwara, H. Idei, A. Iiyoshi, O, Kaneko, K. Kawahata, T. Kawamoto, S. Kubo, T. Kuroda, O. Motojima, V.D. Pustovitov, A. Sagara, C. Takahashi, K. Toi and I. Yamada,
High Beta Experiments in CHS; Sep. 1994 (IAEA-CN-60/A-2-IV-3)

NIFS-304 K. Ida, H. Idei, H. Sanuki, K. Itoh, J. Xu, S. Hidekuma, K. Kondo, A. Sahara, H. Zushi, S.-I. Itoh, A. Fukuyama, K. Adati, R. Akiyama, S. Bessho, A. Ejiri, A. Fujisawa, M. Fujiwara, Y. Hamada, S. Hirokura, H. Iguchi, O. Kaneko, K. Kawahata, Y. Kawasumi, M. Kojima, S. Kubo, H. Kuramoto, A. Lazaros,

R. Liang, K. Matsuoka, T. Minami, T. Mizuuchi, T. Morisaki, S. Morita, K. Nagasaki, K. Narihara, K. Nishimura, A. Nishizawa, T. Obiki, H. Okada, S. Okamura, T. Ozaki, S. Sakakibara, H. Sakakita, A. Sagara, F. Sano, M. Sasao, K. Sato, K.N. Sato, T. Saeki, S. Sudo, C. Takahashi, K. Tanaka, K. Tsumori, H.Yamada, I. Yamada, Y. Takita, T. Tuzuki, K. Toi and T. Watari, *Control of Radial Electric Field in Torus Plasma;* Sep. 1994 (IAEA-CN-60/A-2-IV-2)

NIFS-305 T. Hayashi, T. Sato, N. Nakajima, K. Ichiguchi, P. Merkel, J. Nührenberg, U. Schwenn, H. Gardner, A. Bhattacharjee and C.C.Hegna, *Behavior of Magnetic Islands in 3D MHD Equilibria of Helical Devices*; Sep. 1994 (IAEA-CN-60/D-2-II-4)

NIFS-306 S. Murakami, M. Okamoto, N. Nakajima, K.Y. Watanabe, T. Watari, T. Mutoh, R. Kumazawa and T. Seki, *Monte Carlo Simulation for ICRF Heating in Heliotron/Torsatrons*; Sep. 1994 (IAEA-CN-60/D-P-I-14)

NIFS-307 Y. Takeiri, A. Ando, O. Kaneko, Y. Oka, K. Tsumori, R. Akiyama, E. Asano, T. Kawamoto, T. Kuroda, M. Tanaka and H. Kawakami *Development of an Intense Negative Hydrogen Ion Source with a Wide-Range of External Magnetic Filter Field*; Sep. 1994

NIFS-308 T. Hayashi, T. Sato, H.J. Gardner and J.D. Meiss, *Evolution of Magnetic Islands in a Heliac*; Sep. 1994

NIFS-309 H. Amo, T. Sato and A. Kageyama, *Intermittent Energy Bursts and Recurrent Topological Change of a Twisting Magnetic Flux Tube*; Sep.1994

NIFS-310 T. Yamagishi and H. Sanuki, *Effect of Anomalous Plasma Transport on Radial Electric Field in Torsatron/Heliotron*; Sep. 1994

NIFS-311 K. Watanabe, T. Sato and Y. Nakayama, *Current-profile Flattening and Hot Core Shift due to the Nonlinear Development of Resistive Kink Mode*; Oct. 1994

NIFS-312 M. Salimullah, B. Dasgupta, K. Watanabe and T. Sato, *Modification and Damping of Alfvén Waves in a Magnetized Dusty Plasma*; Oct. 1994

NIFS-313 K. Ida, Y. Miura, S -I. Itoh, J.V. Hofmann, A. Fukuyama, S. Hidekuma, H. Sanuki, H. Idei, H. Yamada, H. Iguchi, K. Itoh, *Physical Mechanism Determining the Radial Electric Field and its Radial Structure in a Toroidal Plasma*; Oct. 1994